Experiments and Direct Dynamics Simulations that Probe η^2-Arene/Aryl-Hydride Equilibria of Tungsten Benzene Complexes

Jacob A. Smith,[1§] Anna Schouten,[2§] Justin H. Wilde,[1] Karl S. Westendorff,[1] Diane A. Dickie,[1] Daniel H. Ess,[2]* and W. Dean Harman[1]*

[1]Department of Chemistry, University of Virginia, Charlottesville, Virginia 22904, United States; [2]Department of Chemistry and Biochemistry, Brigham Young University, Provo, UT 84602, United States. [§] co-first authors.

Abstract.

Key steps in the functionalization of unactivated arenes often involve its dihapto-coordination by a transition metal followed by insertion into the C-H bond. But rarely are the η^2-arene and aryl hydride species in measurable equilibrium. In this study, the benzene/phenyl hydride equilibrium is explored for the {WTp(NO)(PBu_3)} (Bu = n-butyl; Tp = trispyrazoylborate) system as a function of temperature, solvent, ancillary ligand, and arene substituent. Both face-flip and ring-walk isomerizations are identified through spin saturation exchange measurements, which both appear to operate through scission of a C-H bond. The effect of either an electron-donating or electron-withdrawing substituent is to increase the stability of both arene and aryl hydride isomers. Crystal structures, electrochemical measurements, and extensive NMR data, further support these findings. Static density functional theory (DFT) calculations of the benzene-to-phenyl hydride landscape suggest a single linear sequence for this transformation involving a sigma complex and oxidative cleavage transition state. Static DFT calculations also identified an η^2-coordinated benzene complex in which the arene is held more loosely than in the ground state, primarily through dispersion forces. Although a single reaction pathway was identified by static calculations, quasiclassical direct dynamics simulations identified a network of several reaction pathways connecting the η^2-benzene and phenyl hydride isomers, due to the relatively flat energy landscape.

INTRODUCTION

A major frontier of current synthetic-methods research is the functionalization of unactivated C-H bonds.[1-4] For those methods employing π-basic transition-metal catalysts, the key step often involves the insertion of the metal (i.e., oxidative addition), and numerous studies have been carried out on systems that model this process.[5-11] For aromatic molecules, chemoselectivity is a critical issue, not only between sp^2 vs sp^3 (e.g., benzylic) carbons, but between different positions within the aromatic ring. The latter is determined by both thermodynamic and kinetic factors, not only for insertion, but for the binding and migration events that precede it (Scheme 1). Thus, understanding the parameters for these processes, and how each is affected by substituents on the arene (X) and the electronic character of the metal (M) are key to designing high-performance, chemoselective catalysts.

Oxidative addition of an aryl C-H bond is typically thought to occur by the linear sequence of dihapto-coordination followed by C-H σ bond coordination and cleavage to generate an aryl hydride (Scheme 1). This mechanism has been supported by equilibrium observations, and kinetic isotope effects (KIEs) that suggest the existence of intermediates prior to metal insertion into the C-H bond.[12-13] However, in many circumstances it is not known whether the intermediate is exclusively an η^2-arene complex or also a "σ-complex", where the metal straddles the C-H bond. Importantly, Bergman, Parkin, and others have demonstrated that dihapto π coordination is not always a necessary precondition to C-H oxidative addition.[13-14]

Scheme 1. Activation of an aryl C-H bond through binding, migration, and insertion.

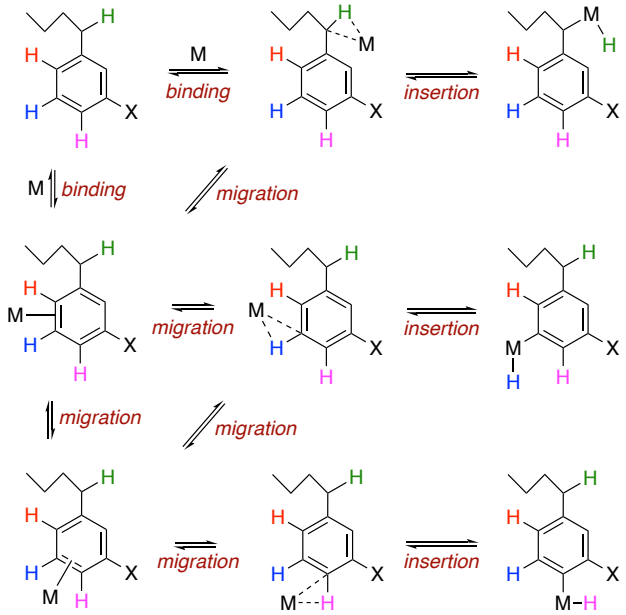

Binding in η^2-arene complexes ranges from relatively weak acid-base adducts[15] to strong metal-arene bonding fortified through significant π-interactions. For the latter case, either the

η^2-arene complex, the aryl hydride, or in rare circumstances an equilibrium of both can be observed, depending on the metal, supporting ligands, and arene substrate.[16-20] For example, Jones showed that at 60 °C, RhCp*(PMe_3)(η^2-naphthalene) exists in a 1:2 equilibrium ratio with RhCp*(PMe_3)(naphthyl)(H).[21-22] This ratio can be altered by adjusting auxiliary ligands or temperature.[22] However, for benzene, only the phenyl hydride was observed. In contrast, the pseudo-octahedral d^6 benzene complexes of $[Os(NH_3)_5]^{2+}$,[23] {ReTp(CO)(L)},[24] and {WTp(NO)(PMe_3)}[17] resist the formation of a seven-coordinate phenyl hydride, and thus η^2-benzene complexes are not only generally observed but are sufficiently stable that organic reactions can be carried out on the bound arene.[17, 23-24] Significantly, in the case of the tungsten complex WTp(NO)(PMe_3)(η^2-benzene), a second set of resonances in the ^{1}H NMR spectrum is observed (~10% of the major isomer) in acetone solution at 0 °C that includes a hydride signal at 9.32 ppm (J_{PH} = 101 Hz; acetone). This feature suggests the presence of an observable η^2-benzene/phenyl hydride equilibrium.[25]

Herein, we report that for the system WTp(NO)(PMe_3)(η^2-benzene), the replacement of PMe_3 by PBu_3 shifts the benzene/phenyl hydride equilibrium from 10:1 to a 1: 2.5 ratio (0 °C), making it an ideal candidate for a more in-depth study of the insertion process. Below, we examine the details of this equilibrium using ^{1}H NMR NOESY experiments and thermodynamic data. Significantly, the hydride resonance corresponding to WTp(NO)(PBu_3)(Ph)(H) is observed to undergo spin-saturation exchange with all six proton resonances of the η^2-arene isomer. Additionally, there is rapid ring-walking around the benzene π framework without a significant KIE or equilibrium isotope effect (EIE). We also explore the effects of various arene substituents (X; Scheme 1), where NOESY experiments reveal a face-flip isomerization process occurring at roughly the same rate as the oxidative addition.

Density functional theory (DFT) calculations are used to outline the energy landscape for the WTp(NO)(PR_3)(η^2-benzene) → WTp(NO)(PR_3)(Ph)(H) (R = Me and Bu) isomerization. These calculations show that on the intrinsic reaction coordinate (IRC)[26] a σ-complex intervenes between the phenyl hydride and η^2-form. Additionally, these static DFT calculations identify a direct π coordination transition state as well as a long-range *noncovalent* W-benzene complex. Because the energy surface for η^2-benzene → phenyl hydride isomerization is relatively flat, and contains several weakly coordinating benzene intermediates, we used DFT quasiclassical direct dynamics simulations to examine transition state connections. This revealed a network of isomerization pathways with non-IRC connections and nonstatistical intermediates.

RESULTS AND DISCUSSION

Synthesis and equilibrium studies.

Using a modified literature procedure,[27] WTp(NO)Br_2 was prepared from $W(CO)_6$ (Scheme 2). Combining WTp(NO)$(Br)_2$ and PBu_3 with zinc dust in a DCM/ether solvent mixture resulted in formation of WTp(PBu_3)(NO)(Br) (**1**). Crystals suitable for X-ray diffraction were grown of this paramagnetic complex via vapor diffusion of ether into a DCM solution of **1**, and details are included in the supplementary material. Infrared and electrochemical data (SI) are similar to those reported previously for WTp(PMe_3)(NO)(Br).[27]

Scheme 2. Synthesis of benzene complex (**2**) and its phenyl hydride isomer (**2H**).

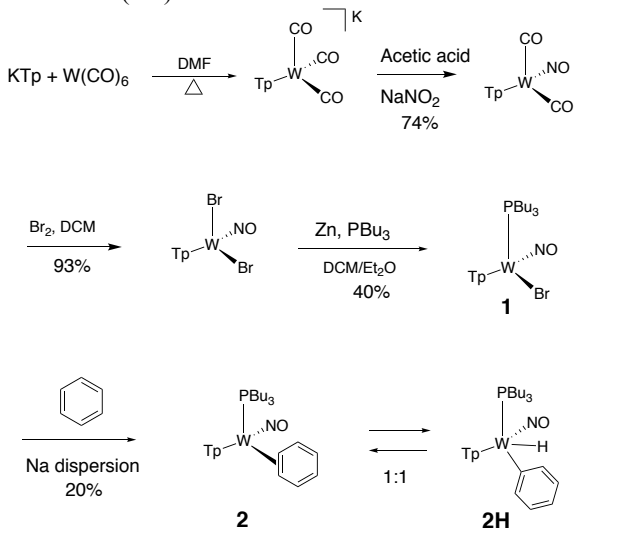

Treatment of **1** with sodium dispersed in benzene yields complex **2**, isolated in 20% yield after chromatography. Complex **2** features an anodic wave in a cyclic voltammogram at $E_{p,a}$ = -0.16 V, which is consistent with data collected for the η^2-bound benzene complex WTp(NO)(PMe_3)(benzene) (cf. -0.13 V).[27] ^{1}H NMR analysis confirmed the identity of **2** as WTp(NO)(PBu_3)(η^2-benzene) in solution. However, a second set of NMR signals of equal intensity indicated the presence of the phenyl-hydride isomer WTp(NO)(PBu_3)(H)(Ph) (**2H**). Notably, **2H** features a hydride doublet at 9.62 ppm (J_{PH} = 97.3 Hz) that is accompanied by ^{183}W satellites (J_{WH}= 32.1 Hz). At 25 °C, **2** has a substitution half-life ($t_{1/2}$ =4 min) that is significantly less than its PMe_3 complex (cf. $t_{1/2}$ = 66 min).[27] A weak IR absorption observed at 1989 cm^{-1} (cf. DFT prediction 1988 cm^{-1}) taken of an isolated solid of **2**/**2H** is tentatively assigned to a W-H vibrational mode. Even as a solid stored at -30 °C under inert atmosphere, the **2**/**2H** mixture decomposes to uncharacterized paramagnetic materials after several weeks.

The equilibrium ratio of **2**:**2H** in benzene-d_6 is 1:1. When the isolated solid of **2**/**2H** obtained from an ether/pentane precipitation is added to a cold solution (~10 °C) of benzene-d_6 and monitored, an initial ratio of **2**:**2H** of 1:3 was observed, which over time returned to a 1:1 ratio. While these observations suggest that the solid was enriched in the hydride isomer, attempts to grow crystals of **2H** suitable for X-ray diffraction were unsuccessful.

To better understand the mechanics of the **2**/**2H** conversion, we carried out ^{1}H NMR NOESY experiments of this mixture as an acetone-d_6 solution at 0 °C (Figure 1). The η^2-benzene complex (**2**) shows spin-saturation exchange with the phenyl hydride (**2H**), indicating that these two species are in dynamic equilibrium. Specifically, the tungsten-hydride proton

undergoes chemical exchange with every benzene ring proton of the dihapto-coordinated isomer, demonstrating that interconversion between **2** and **2H** occurs on the seconds timescale at 0 °C. An exchange process was also detected between the benzene hydrogens in **2**. A similar ring-walk was observed for the PMe_3 analog (0 °C).

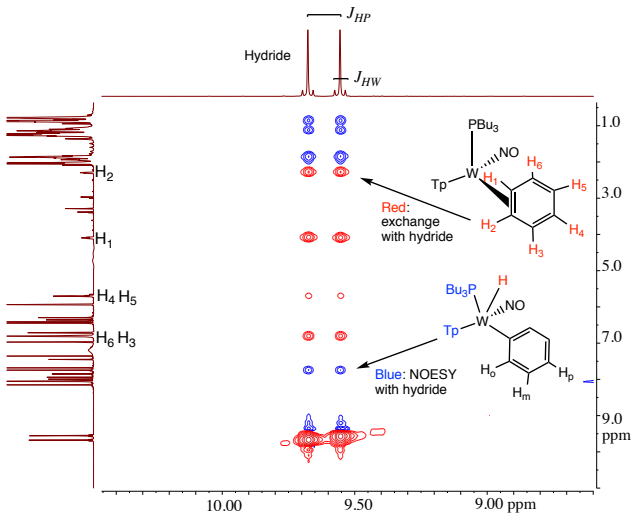

Figure 1. ^{1}H NMR spectrum of the hydride region and its NOESY correlations of **2**/**2H**.

Using the H_1 proton for **2** and line-broadening techniques, $\Delta G^{\ddagger}$ for proton exchange *within* **2** was determined to be 16 ± 2 kcal/mol (35 °C). Similar correlation intensities in the NOESY data for both the benzene ring-walk (e.g., H_1 of **2** <=> H_6 of **2**) and phenyl hydride (e.g., W-H of **2H** <=> H_1 of **2**) exchanges suggest that these rates are similar if not identical. Using Tp4 protons that distinguish **2** from **2H**, a free energy of activation ($\Delta G^{\ddagger}$) for the conversion of **2** to **2H** was determined to be 15 ± 2 kcal/mol (at the coalescence temperature of 44 °C). This value is similar to that determined for the ring-walk of **2**, and suggests that the ring-walk process may involve C-H insertion (Scheme 3). However, the available data cannot rule out an alternative mechanism in which the tungsten moves from 1,2-η^2 to 2,3-η^2 *without* insertion into a C-H bond. This "ring-slip" pathway (i.e., an intrafacial isomerization) is shown in Scheme 3 for comparison. We note that NOESY data recorded for the deuterated analog WTp(NO)(PBu_3)(η^2-benzene-d_6) (**2-*d*$_6$**) show correlation intensities resulting from exchange for the Tp ring protons that appear practically identical to what was observed for **2**. This observation indicates that there is not a major kinetic or thermodynamic isotope effect for the oxidative addition process.

Static DFT landscape for the C-H insertion

NOESY experiments established the dynamic equilibrium of the η^2-benzene (**2**) and phenyl hydride (**2H**) complexes. Because the measured barriers are similar for ring-walk in the η^2-benzene complex (**2**) and its conversion to the phenyl hydride complex (**2H**), this measurement was not able to determine if the ring-walking mechanism occurs only via an oxidative addition and reductive elimination sequence or if there is also a ring-slip mechanism in play. Additionally, the timescale of the NMR experiments is too long to capture key intermediates that may be only briefly sampled during the exchange process. Therefore, we used DFT calculations to explore intermediate and transition-state structures that connect the η^2-benzene (**2**) and phenyl-hydride (**2H**) complexes.

Scheme 3. Isomerization and spin-saturation-exchange (represented by blue, green, red, and pink colored hydrogens) for the phenyl hydride complex (**2H**) and its benzene isomer (**2**).

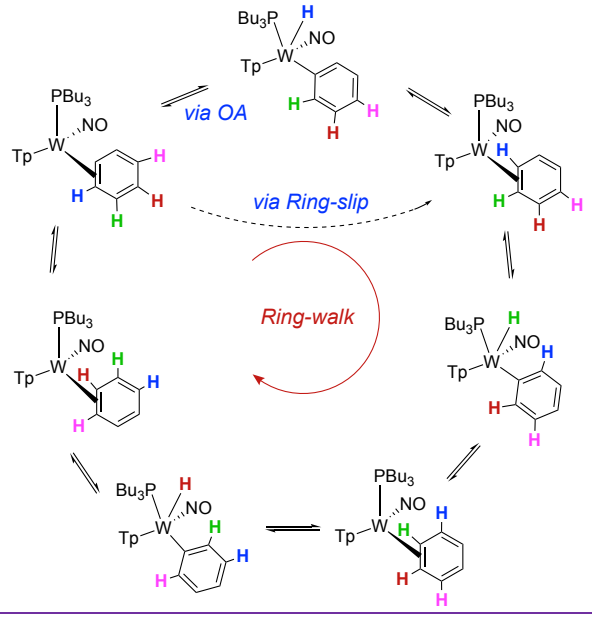

All stationary points were optimized with M06[28] and M11[29] functionals using the 6-31G**[LANL2DZ for W] basis set in Gaussian 16.[30] These functionals were chosen because they provide accurate evaluation of the experimental isomerization energies and structures (see discussion below). Structures were confirmed as minima or transition states by vibrational frequency analysis. All transition-state structures have a single negative vibrational frequency. Rigid-rotor-harmonic-oscillator thermochemical corrections at 298 K and 1 atm were added using the default implementation in Gaussian 16. Optimizations and single point calculations were performed using the SMD[31] continuum solvent model for acetone, which provided an estimate of ΔG_{solv} that was added to gas-phase enthalpy and Gibbs free energy values.

The static enthalpy and Gibbs energy landscape for WTp(NO)(PMe_3)(η^2-benzene) in equilibrium with WTp(NO)(PMe_3)(H)(Ph) is displayed in Figure 2. The **2** and **2H** labels were used for PMe_3 structures. A comparison of the M06 W-C bond lengths calculated for **2** with the SC-XRD-determined values for WTp(NO)(PMe_3)(η^2-benzene)[32] show excellent agreement (within 0.01Å; Figure 3). For M06, the ΔG value between **2** and **2H** is 2.3 kcal/mol, which is within reasonable accuracy of the experimental value for a 10:1 ratio

of benzene/hydride (= 1.37 kcal/mol @ 25 °C). Use of a larger basis sets, such as Def2-TZVP, changes this Δ*G* value by less than 0.5 kcal/mol (see SI). The M11 functional gives an even closer Δ*G* value of 0.7 kcal/mol.

In order to test the validity of modeling the PBu_3 system as the less complex PMe_3 system, we also calculated the energy difference between WTp(NO)(PBu_3)(η^2-benzene) and WTp(NO)(PBu_3)(H)(Ph) for comparison. For M06, Δ*H* and Δ*G* are 2.4 and 0.1 kcal/mol respectively, which is extremely close to representing the ~1:1 ratio of **2**:**2H** with PBu_3. M11, is also close, but slightly overestimates the stability of the phenyl complex with a Δ*G* value of -1.4 kcal/mol. From either set of calculations, the replacement of methyls for butyls stabilizes the aryl hydride both entropically and enthalpically (vide infra). While these structures and calculations are not represented in the text, they are available in the SI.

Regarding the phenyl-hydride complex **2H** shown in Figure 3, a second isomer is possible in which the hydride and phenyl groups are transposed. That isomer is roughly 6 kcal/mol higher in enthalpy and its structure and associated transition states are summarized in the SI, but not considered further. Similarly, we located the conformational isomer to **2**, **2-endo**, that is 4 kcal/mol higher in energy where the benzene ring projects over the Tp ligand rather than the NO group.

A reductive coupling transition state **TS1** was located with a M06 enthalpy barrier of 12.0 kcal/mol and a Gibbs free energy barrier of 10.5 kcal/mol, relative to **2H**. As expected, this transition state features lengthened W-Ph (2.91 Å) and W-H (2.36 Å) bonds along with simultaneous, but very advanced (i.e. geometrically "late"), formation of the C-H bond (1.11 Å) (Figure 3). IRC calculations indicate that **TS1** connects **2H** to the intermediate **2σ**, which is a C-H σ-complex. **TS1** and **2H** are geometrically very similar. Furthermore, the energy surface surrounding **TS1** and **2σ** is extremely flat. **2σ** is < 1 kcal/mol lower in enthalpy and ~2 kcal/mol lower in Gibbs energy than **TS1**. In addition, surrounding **2σ**, we located transition state **TS2** with a negative vibrational frequency of -70 cm^{-1} and IRC calculations suggest connection with the η^2-benzene complex **2** through a rotational motion. **TS2** has a Gibbs barrier of only 2.1 kcal/mol relative to **2σ**, and the enthalpy of **TS2** is slightly lower than **2σ**, indicating that that sigma complex is in a very shallow energy well.

Geometrically, relative to **2**, **TS2** shows greatly elongated W-C bonds (2.67 and 3.18 Å, cf. 2.23, 2.26 Å for **2**), as well as a weak W-H interaction (2.93 Å), and virtually no change to the C-H bond (1.09 Å). Hence, the transition from **2σ** to **TS2** could be described as the benzene beginning to dissociate from the metal and rotating the ring to bring the subject C-H bond roughly parallel to the HOMO of the {WTp(NO)(PMe_3)} fragment (i.e. parallel to the W-P bond axis).[33] Because **TS2** has geometric character of benzene dissociation and arene rotation there is the possibility of non-IRC connections through this transition state, which will be discussed later.

From **2**, transition states **TS1** and **TS2** have M06 free-energy barriers of 12.8 and 12.7 kcal/mol, respectively.[34] Both of these barriers are close to the experimental range for the free energy barrier estimate (15 ± 2 kcal/mol at 44 °C), which provides confidence that this DFT method provides an accurate representation of the energy surface. While M11 gives a slightly more accurate value for the **2** and **2H** energy difference with PMe_3, it underestimates the **TS1** and **TS2** barriers by ~5 kcal/mol (see SI). All other functionals examined did not have as good of performance compared to M06 (see SI). We note that **TS2** and **2σ** are several kcal/mol lower than full dissociation on the enthalpy surface, and experimentally, **2H** and **2** interconvert many cycles without being displaced by acetone solvent ($t_{1/2}$ = 4 min for **2** and 66 min for the PMe_3 analog at 25 °C).[32] This comparison with experiment suggests that the Gibbs energy of separated benzene and {WTp(NO)(PMe_3)} should probably not be compared with the Gibbs energy of **TS2** and **2σ** using standard approximations since the translational entropy is likely overestimated.[35]

Figure 2. M06/6-31G**[LANL2DZ] enthalpy and Gibbs (in parentheses) landscape for isomerization of phenyl hydride to η^2-benzene complex. M11/6-31G**[LANL2DZ] values are given in bracketed italics. The PBu_3 groups of **2** and **2H** were modeled as PMe_3. Energies are reported in kcal/mol. Red: IRC connections for phenyl group rotation, reductive coupling, sigma to η^2-arene isomerization, and partial benzene dislocation to **2π**.

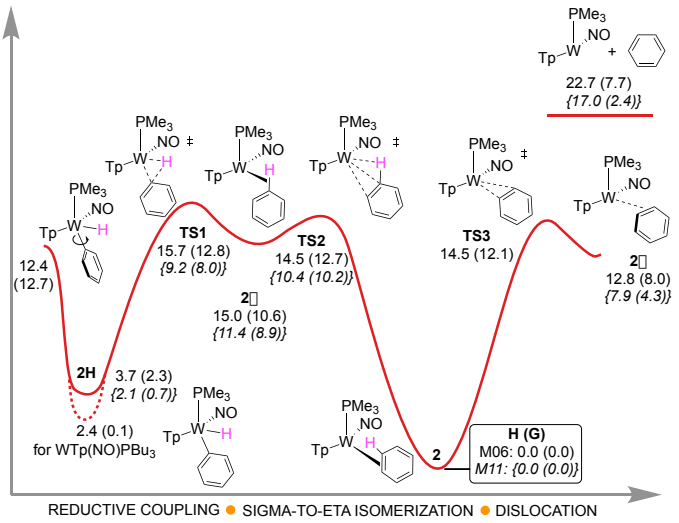

We also located the transition state for the W-Ph bond rotation of **2H**. The enthalpy and Gibbs barriers for this process from **2H** are 8.7 and 10.4 kcal/mol, which are lower than **TS1** which indicates rapid W-Ph rotation compared to reductive coupling. Hence, this sequence provides a mechanism for *interfacial* isomerization (face-flip), as well as a ring-walk (*vide infra*).

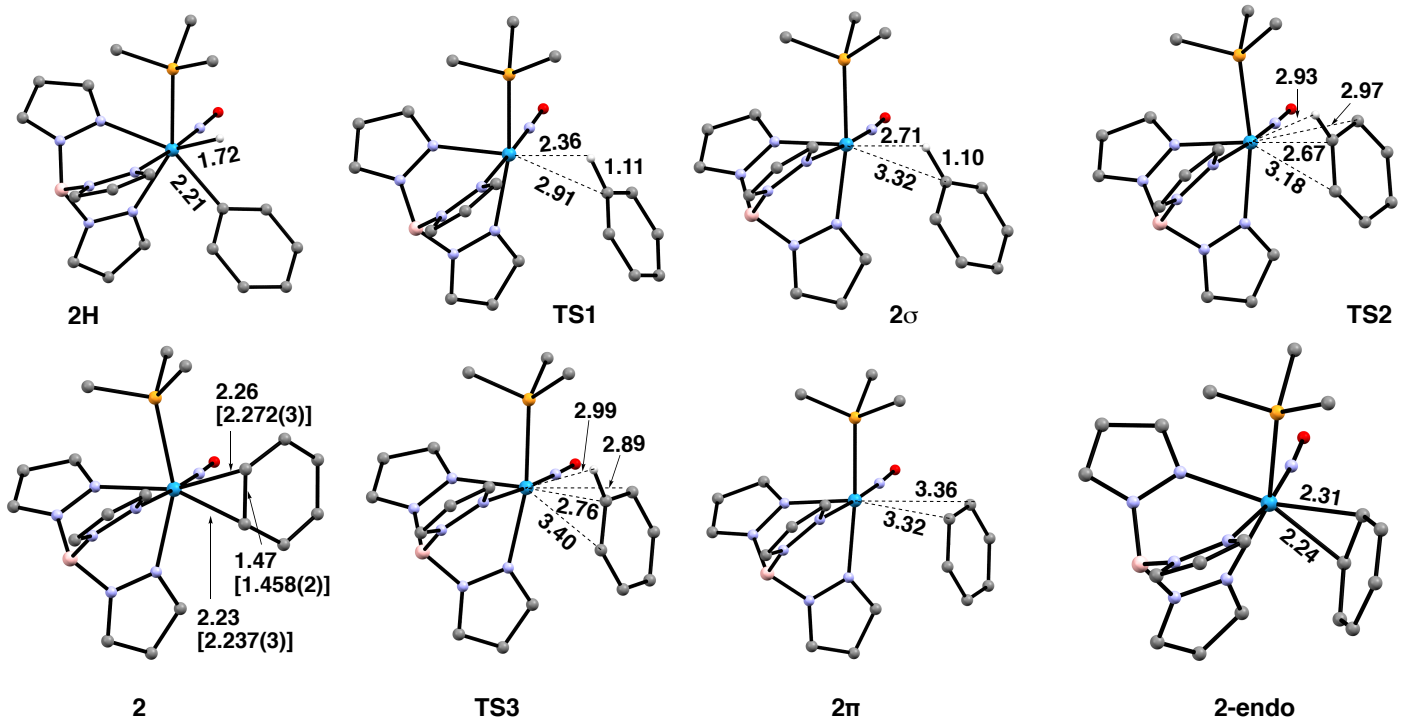

Figure 3. M06 derived ground state, intermediate, and transition-state structures for WTp(NO)(PMe$_3$)(η^2-benzene) and WTp(NO)(PMe$_3$)(H)(Ph) isomerization. The PBu$_3$ groups of **2** and **2H** were modeled as PMe$_3$. Distances reported in Å. red = O; blue = N; orange = P; pink = B. Bracketed bond distances for structure **2** represent SC-XRD data (ref. 32).

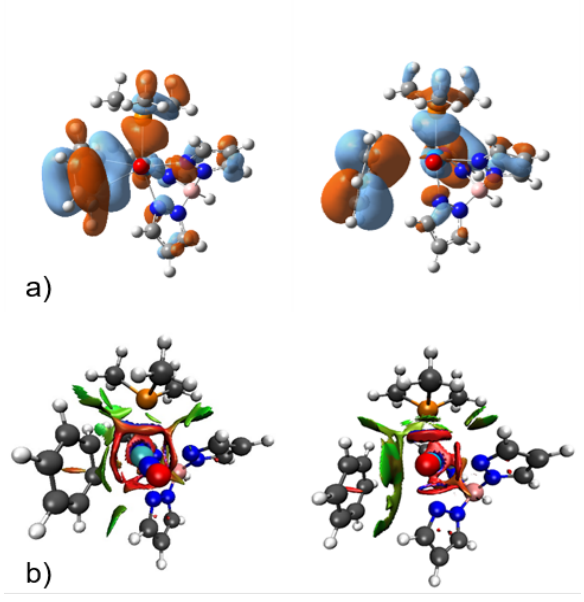

Figure 4. a) M06-derived molecular orbitals (**2**: HOMO-3; **2π**: HOMO-4), and b) NCI plot comparisons of WTp(NO)(PMe$_3$)(η^2-benzene) (**2**) with the elongated WTp(NO)(PMe$_3$)-benzene complex (**2π**).

In addition to locating the stationary points connecting **2H** and **2**, we also searched for structures that could potentially describe direct benzene coordination/dissociation to/from {WTp(NO)(PMe$_3$)}. With M06 we located transition state **TS3** (Figure 2 and Figure 3) where the negative vibrational frequency of -106 cm^{-1} indicates motion directly to and from the W metal center. While IRC calculations confirm that in one direction **TS3** connects to a η^2-benzene complex, the opposite direction was not definitive due to errors in the calculation, even with extremely small step sizes, presumably due to the flatness of the energy surface for benzene dissociation. It is unlikely that **TS3** connects to separated benzene and {WTp(NO)(PMe$_3$)} because these species are ~8 kcal/mol higher in enthalpy than **TS3**. Also, in **TS3** the benzene approaches the tungsten with the interacting C-C bond parallel to the W-NO axis, and this orientation is perpendicular the benzene orientation in **2**.

Because it is unlikely that **TS3** connects to separated benzene and {WTp(NO)(PMe$_3$)}, we searched for another possible WTp(NO)(PMe$_3$)-benzene complex. This led to the location of the weak coordination complex **2π**. In this complex, the W-C interaction distances are 3.32 and 3.36 Å (Figure 3), the C-C bond lengths within the aromatic ring are all roughly equal to the free aromatic (1.39 Å), and the C-C axis of the bound carbons, like **TS3**, is parallel to the W-NO axis. In contrast, for **2** the C-C axis is parallel to the W-P axis in order to maximize the backbonding interaction with the HOMO of {WTp(NO)(PMe$_3$)}, i.e., the dπ orbital that does not interact with the nitrosyl ligand. These features suggested to us that the

η^2-benzene complex **2** is a tight charge-transfer (orbital) interaction complex with bonding and backbonding interactions, while **2π** is likely held together through dispersion interactions. We also confirmed that this structure can be located using DFT methods with an explicit dispersion term (see SI). Figure 4a shows that only in the η^2-arene complex is there significant frontier orbital overlap between benzene and the W metal center. Figure 4b compares the noncovalent interaction plots using NCIplot[36] between these two complexes. This shows that the noncovalent interaction significantly increases as the W-benzene distance increases. An energy decomposition analysis using the absolutely localized molecular orbital (ALMO) method in Q-Chem confirmed that 2/3 of the W-benzene interaction in **2π** is due to dispersion.[37-38] In contrast, in **2** charge transfer orbital interactions dominate the interaction stabilization (see SI for values).

Quasiclassical direct dynamics simulations

While the energy landscape connecting the phenyl hydride **2H** with the η^2-benzene **2** indicates that there is an intervening σ-complex intermediate (**2σ**) and a **2σ** → **2** isomerization transition state (**TS2**, Figure 2), the flat shape of this surface suggests that there might be non-IRC motion and nonstatistical population of structures through the lack of internal vibrational energy redistribution (IVR). Also, IRC calculations were not definitive about the connection from **2** going through **TS3**, which is very close to **TS2** in both energy and structure. Therefore, we carried out quasiclassical trajectory calculations with M06/6-31G**[LANL2DZ]. We also carried trajectories with the M11 functional for comparison. M06/6-31G**[LANL2DZ] provides an accurate representation of the relative energies of structures compared with experiment. Trajectories were initialized and propagated in forward and reverse directions from all transitions states using normal mode and thermal sampling that included zero-point energy at 273 K. Trajectories were propagated forward and reverse in mass-weighted Cartesian velocities with an approximate time step of 1 femtosecond (fs).

This trajectory analysis revealed several unexpected non-IRC connections where a transition state can lead to multiple products in each direction[39] The SI gives detailed categorization of all trajectories. Scheme 4 outlines all the unique reaction trajectories that proceed through **TS1**, **TS2**, and **TS3** along with the relative percentage of each pathway that utilize each of these transition states. Figure 5 offers a multidimensional model representation to visualize the network of pathways that the dynamics simulations reveal.

On the static energy surface shown in Figure 2, IRC calculations indicate that **TS1** connects the phenyl hydride with **2σ**. We propagated 42 M06 trajectories in the forward and reverse directions starting at **TS1**. 25 trajectories connected energy minima passing through **TS1** while 17 trajectories showed recrossing. In accord with this IRC perspective, all trajectories connect **TS1** with **2σ**. 86% of all trajectories showed **2H** → **TS1** → **2σ** connection (*red path*, Figure 5, Scheme 4). Re-crossing trajectories were not considered in the relative percentages of reaction pathways reported in Scheme 4. With 24 additional M11 trajectories, we also found the majority of trajectories with this IRC connection (see SI). For the direction of **TS1** → **2H**, we did not generally observe W-Ph bond rotation and therefore this rotation is not coupled with the reductive coupling process. Unanticipated, approximately 14% of trajectories showed **TS1** connecting the σ-complex (**2σ**) and the η^2-benzene complex (**2**), *without* passing through **TS2** (*red and dark green paths*, Figure 5). This demonstrates that the weak σ-complex, **2σ**, and the energy surface surrounding it, provides a pathway branching area for reductive coupling/oxidative cleavage and π coordination. M11 trajectories also showed branching at **2σ**, but different than M06 trajectories ended at **2π** rather than **2**.

The static DFT surface (Figure 2) indicates that **TS2** is slightly lower in energy than **TS1**. Therefore, during the **2H** → **2** isomerization process **2σ** will not only return to **TS1** but will also achieve **TS2**. While on the static surface the IRC suggests that **TS2** connects **2σ** with **2**, the energy surface surrounding **TS2** is flat (orange-colored surface area in Figure 5) and dynamical effects are likely to impact pathways leading to and from **TS2**. Indeed, our 56 M06 trajectories revealed five unique reaction pathway connections that involve **TS2**, which are outlined in Scheme 4 and Figure 5. Importantly, the five connections shown in Scheme 4 include the first major connection for **TS2**: **2σ** to **2π**. Many of the structures arrived at from **TS2** evolved further. For example, some trajectories showed the ring alternating between a given **2σ** and **2π** (*red and yellow paths*) structure, while other trajectories evolved as a sequence of different **2σ** and **2π** structures such that multiple carbon and hydrogen atoms encounter the tungsten metal center (analogous to the ring walk of the η^2-arene **2**). Similar to M06, 50 trajectories with M11 showed all the same major dynamical pathways with **TS2**, although not in the same quantitative ratio due to the limited number of trajectories possible to propagate with a very large system (see SI).

Scheme 4. Outline of M06 trajectory connections to and emanating from **TS1**, **TS2**, and **TS3**. Percentages are the relative amount of each pathway that utilize these transition states, and do not include re-crossing.

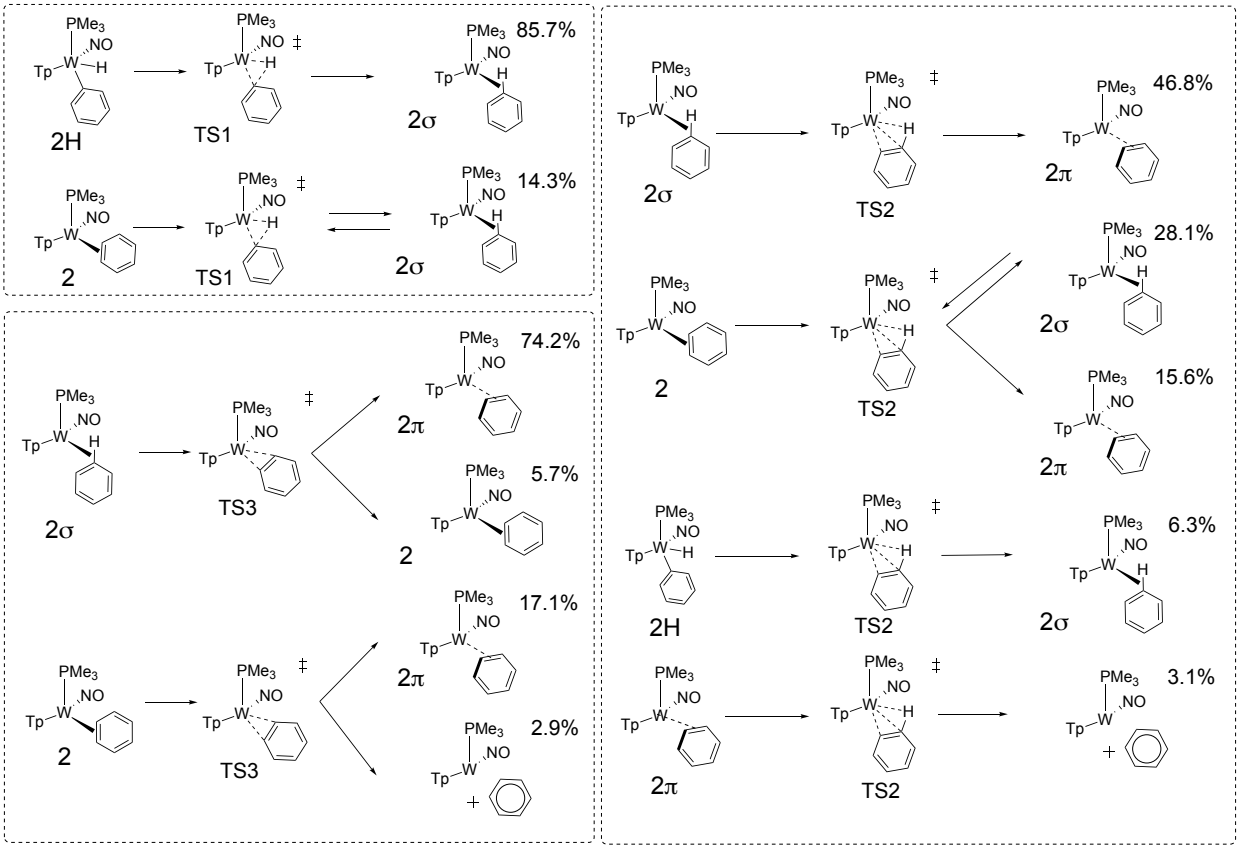

Unexpectedly, the major reaction pathway that accounts for ~50% of the trajectories for **TS2** involves the non-IRC conversion of **2σ** to **2π** (*red and yellow paths*, Figure 5), rather than the η^2-arene **2**. This dynamical connection is reasonable considering the geometry of **TS2**. As stated previously, while the negative vibrational frequency of **TS2** shows mostly rotation of the arene, the W-C distances are very long and potentially closer to **2π** than **2**. While the most important result is the general pathway branching identified through **TS2**, and these results were modeled in continuum solvent, it is possible that modeling with explicit solvent might alter the percentage of branching towards **2** versus **2π**, and the percentages through **TS2** should be interpreted qualitatively. This interpretation is especially important due to the limited number of trajectories that are able to be examined with this very large system. However, it is not obvious if explicit solvent would diminish or enhance directing trajectories from **TS2** towards **2π**, especially because the timing of solvent translation is significantly longer than the 500-750 fs time scale of traversing through the **TS2** zone.

The next significant trajectory pathway for **TS2** accounts for >25% of trajectories and is the IRC-identified **2σ** → **2** pathway. This pathway along with its microscopic reverse provides a mechanism for an intrafacial ring-walk isomerization (ring-slip) that does not require C-H cleavage. Roughly similar in magnitude, ~15% of the trajectories connected **2** → **TS2** → **2π**. This connection is outlined in Figure 5 with a *red* path from **2** to **TS2** and then *yellow* from **TS2** to **2π**. This connection of **2π** with **2** is perhaps not surprising since the W-π_{CC}* interaction in **2** is significantly stronger than W-σ_{CH}* interaction in **2σ**.

Two other pathways account for ~10% of the trajectory connections. The small amount of these trajectories should be cautiously interpreted, especially since trajectories were not found with the M11 functional. These two trajectory pathways include **2H** → **TS2** → **2σ** (*black and red*, Figure 5) and **2π** → **TS2** → [{WTp(NO)(PMe_3)} + benzene] (*yellow and dusty rose paths*, Figure 5). This later reaction pathway leading to benzene dissociation was unexpected and, similar to connections to **2π**, might be significantly influenced by explicit solvation spheres. Again we note, however, that the experimental rate of benzene ring-walking (seconds timescale) is much faster than for benzene displacement by either benzene-d_6 or acetone-d_6 (hours timescale).

The static DFT surface indicates that when the η^2-benzene complex **2** is formed there is a nearly equal barrier for going towards **TS2** (*red path*, Figure 5) as there is to achieve **TS3** (*dark blue path*, Figure 5). This suggests that during the isomerization process **TS3** will also be sampled. We propagated 52 M06 trajectories through **TS3**. 35 trajectories showed forward and reverse connections while 17 showed recrossing. Perhaps unexpected, for the fully connected reactive trajectories, the major pathway shown for **TS3** in Scheme 4 is

2σ → **TS3** → **2π** (*light blue* and *magenta paths*, Figure 5), which accounts for nearly 75% of all connections. Only 17% of the trajectories connect the η²-benzene complex **2** with **2π** through **TS3** (*dark blue* and *magenta*). This indicates that **TS3** should perhaps not be interpreted as a direct π coordination transition state, but rather a general coordination transition state where collisions can lead to either σ (*light blue path*, Figure 5) or π (*dark blue path*, Figure 5) type coordination. Also important, similar to trajectories for **TS2**, trajectories from **TS3** moved through other intermediates after arriving at either **2σ** or **2π** and occasionally continued on to **2** or **2H**.

Overall, the static DFT calculations suggest that during the isomerization process there is access to **TS1**, **TS2**, **TS3**, and possibly other intermediates and transition states, all roughly 4 kcal/mol below complete dissociation. The dynamics trajectories further revealed all of these transition states provide a complex network for interconversion of **2H** with **2σ**, **2**, and **2π**, as illustrated in Figure 5. Significantly, the direct connection between **2H** and dissociation (either via **TS2** or **TS1** and **TS3**) indicates by the principle of microscopic reversibility that η²-coordination is not necessary for insertion into the C-H bond.[25] Finally, we note that while these calculations indicate pathways for ring-walking that do not require C-H oxidative addition (i.e., a ring-slip), the same is not true for face-flipping, which appears to require C-H scission followed by rotation of the phenyl-W bond.

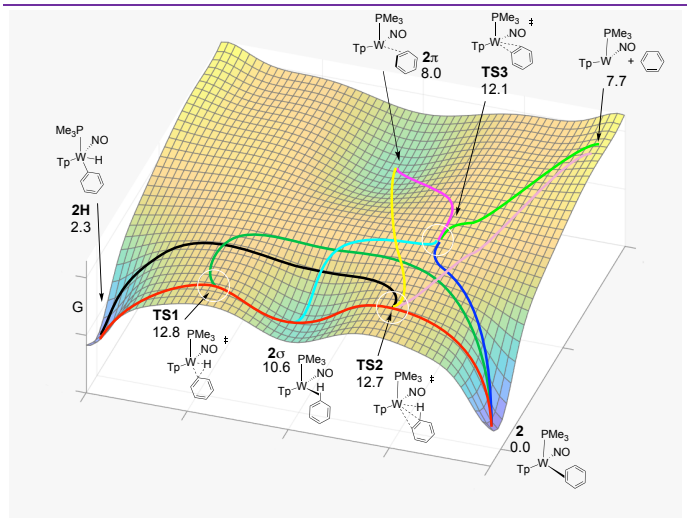

Figure 5. A representation of the reaction coordinate network (Gibbs) connecting **2H**, **2**, **2σ**, and **2π**.

Substituent effects

We next set out to determine how a substituent on the benzene ring affects the η²-benzene/phenyl-hydride equilibrium, as well as how it affects the regioselectivity of these species. We began by examining the role of a π-donor group (OMe). Reduction of **1** with sodium dispersion in neat anisole led to the formation of WTp(NO)(PBu₃)(anisole) (**3**), isolated as a 4:1:1 mixture of two η²-arene complexes **3A** (4) and **3B** (1), along with an aryl hydride species ***m*-3H** (1) (Scheme 5). We note this behavior is in contrast to what is typically observed for anisole.[40] Close examination reveals a minor amount of a second hydride complex (0.1) that we tentatively assign as ***o*-3H** (0.1), based on its chemical exchange with **3A** and **3B** (vide infra). Parenthetically, the anisole complex **3** can be prepared on a 15 g scale at 50% yield, a value comparable to that of the {WTp(NO)(PMe₃)}analog.[27] This complex is stable for months while stored as a solid at low temperatures (-30 °C). The substitution half-life of **3** at 25 °C is ~ 20 minutes, making it a suitable synthon for {WTp(NO)(PBu₃)}, especially in cases where a potential ligand is incompatible with the reducing capability of sodium.

NOESY data for an acetone solution of **3** indicate chemical exchange between all four anisole complex isomers in solution (**3A**, **3B**, ***o*-3H**, ***m*-3H**; Scheme 5). Significantly, the only exchange observed between meta protons of the various isomers is H₃ of **3A** with H₃ of **3B** and the hydride of ***m*-3H**. Likewise, H₂ of **3A** exchanges with H₂ of **3B** and the weak hydride signal of ***o*-3H**. However, there is no exchange between the *ortho* proton H₂ in **3A** with the ortho proton H₆ in either **3A** or **3B**, nor do the hydride signals exchange with H4 of either **3A** or **3B**. Although signals for the minor species ***o*-3H** are far too weak to fully characterize it, based on the chemical exchange of the hydride signal, we can confidently rule out this compound being the para hydride (***p*-3H**).

Scheme 5. The interconversion of **3A** and **3B** occurs through C-H insertion for anisole complex **3**. Blue and pink colored hydrogens indicate observed or expected spin saturation exchange for each mechanism.

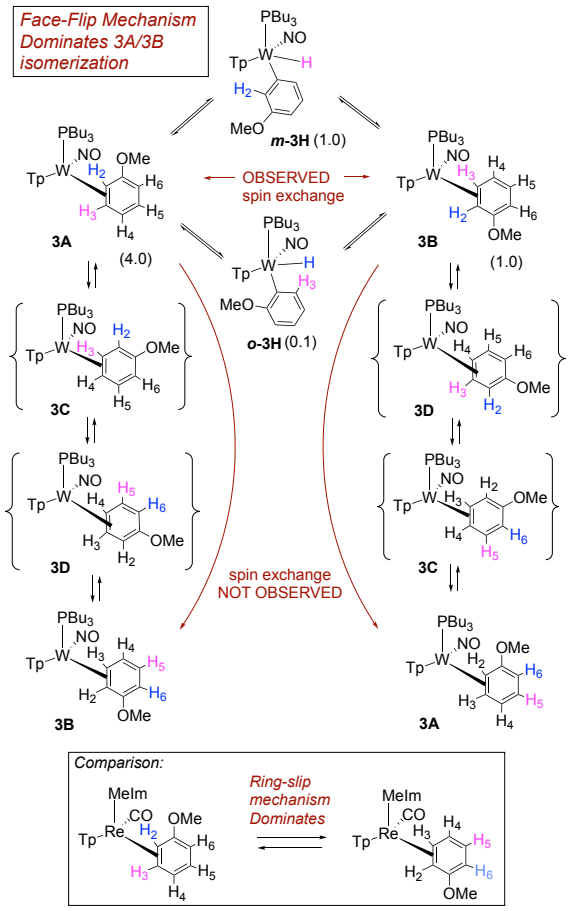

These observations above indicate that for the η^2-anisole diastereomers, the interconversion of **3A** and **3B** occurs via a face-flip (interfacial) isomerization, which must be significantly faster than a purported ring-slip (intrafacial isomerization). This is in contrast to that observed for the complex ReTp(CO)(MeIm)(η^2-anisole), (MeIm = N-methylimidazole) which undergoes intrafacial isomerization (ring-slip) roughly four times *faster* than interfacial isomerization (face-flip; Scheme 5).[41]

Possible mechanisms for both face-flip and ring-walk isomerization for the anisole complex were examined with DFT, and an abbreviated energy surface with π and W-H complexes is shown in Figure 6. Consistent with experiment, the meta aryl hydride ***m*-3H** is 1.9 kcal/mol lower in Gibbs free energy than the ortho counterpart ***o*-3H**. However, as with benzene (**2**; Figure 2), both species are calculated (using PMe_3) to be significantly higher in Gibbs free energy than the dominant 2,3-η^2 isomers (**3A** and **3B**; Figure 6). Another important comparison to experiment is that the M06 calculations show **3A** and **3B** to have nearly identical Gibbs energy values and **3B** to be only 0.8 kcal/mol endothermic relative to **3A**. Both of these values are consistent with the 4:1 ratio of **3A**:**3B** found experimentally.

Calculations indicate that the 3,4-η^2 isomers (**3C**, **3D**) are 4-6 kcal/mol less stable (based on Gibbs energies; 6-4 kcal/mol more endothermic) than the 2,3-η^2 counterparts (**3A**, **3B**). There are two explanations for the difference in ground energies of **3A**/**3B** compared to **3C**/**3D**. First, metal coordination partially dearomatizes the system leaving a 1,3-diene system. For **3A**/**3B**, the OMe group is in linear-conjugation while in **3C**/**3D** the OMe group is in cross-conjugation (see the *uncoordinated* portion in red below).[42] This notion is supported in the calculated C-O bond lengths for **3A** (1.360 Å) and **3B** (1.358 Å), which are shorter than for **3C** (1.364 Å) and **3D** (1.364 Å). For comparison, a SC-XRD study of **3A** shows a C-O bond length of 1.336 Å (SI); cf. free anisole: 1.373 Å (SC-XRD)).[43] Additionally, DFT analysis of 1-methoxycyclohexa-1,3-diene versus 2-methoxycyclohexa-1,3-diene shows an enthalpy difference of 2.5 kcal/mol. A second explanation is that the anisole π to W-d_σ donor interaction is enhanced at the ortho position compared to the para position, which is consistent with the nodal properties of the occupied anisole π orbitals (see SI).[44] The difference in orbital, charge-transfer interactions was confirmed using the ALMO method.

The blue pathway in Figure 6 shows that for **3A** the oxidative cleavage transition state, ***o*-TS1**, has a Gibbs barrier of 12.7 kcal/mol and results in the W-H ***o*-3H**. The σ-complex intermediates (***o*-3σ**, ***m*-3σ**, ***p*-3σ**), and σ to π transition states (***o*-TS2, *m*-TS2, *p*-TS2**) are not shown on this energy surface. From ***o*-3H** it could be possible for W-aryl bond rotation followed by reductive coupling to lead to **3B**, which constitutes a face-flip mechanism. However, due to the congestion of the aryl OMe group, the Gibbs barrier for rotation (shown as dotted lines) is 22.1 kcal/mol. Instead, the red pathway in Figure 6 through either complete or partial ring-walking provides a lower energy route for conversion, shown as beginning with **3B**. From **3B** there is a meta oxidative cleavage transition state, ***m*-TS1**, with a Gibbs barrier of 15.6 kcal/mol. This is similar to ***o*-TS1**, but lower than the rotation barrier in the blue pathway. The ***m*-TS1** is higher than **TS1** of the benzene complex, which is consistent with higher barriers and slower isomerization for trifluorotoluene (vida infra).

Interestingly, for both the ortho and para hydrides (***o*-3H**, ***p*-3H**), the first transition state (***o*-TS1-short** and ***p*-TS1-short**) varied considerably from the **TS1** of benzene (Figure 6), and in the case of para, this transition state lead to a corresponding "short" sigma complex (***p*-3σ-short**). A second transition state (***p*-TS1**) and sigma complex (**p-3σ**) were also located, that more closely resembled those of benzene (**TS1** and **2σ**). For ***o*-TS1-short** and ***p*-TS1-short** the C-H insertion is significantly more developed than in the more loosely-bound **TS1** transition states, with longer C-H bonds (***o*-TS1**: 1.31 Å; ***p*-TS1**: 1.28 Å), and shorter W-C bonds (***o*-TS1**: 2.27 Å; ***p*-TS1**: 2.27 Å), compared to their benzene counterpart (**TS1**: C-H = 1.11 Å and W-C = 2.91 Å). We speculate that a sigma complex similar to ***p*-3σ-short** likely exists for the ortho hydride as well (***o*-3σ-short**) but this was not located. These "short" sigma complexes and accompanying transition states were not located for the meta hydride, which evolved directly into ***m*-TS1** (C-H = 1.11 Å and W-C = 2.83 Å) and ***m*-3σ**. Apparently, the π-donating property of the methoxy group provides the extra electron-density in the ortho and para C-H bonds to stabilize the more conventional tightly bound sigma complexes, which then evolve into their loosely bound counterparts (***o*-3σ**, ***p*-3σ**; Figure 6). See the SI for a more in-depth discussion on anisole transition states and σ-complexes.

Importantly, from ***m*-3H** there is the possibility of either continued ring walking around the ring through oxidative cleavage/reductive coupling, or W-aryl bond rotation, either of which would eventually lead to **3A**. At ***m*-3H** the W-aryl bond rotation barrier is only 15.1 kcal/mol. We note that the relative energy of ***p*-3H** compared to ***o*-3H** and ***m*-3H** suggests that it should be a minor species and observed in similar quantity to ***o*-3H**. However, experiments did not detect ***p*-3H**. While this might indicate that the traversing through **3C**, **3D**, ***p*-TS1**, and ***p*-3H** (i.e., a complete ring-walk) does not occur as rapidly as the face-flip mechanism, none of the transition state barriers are sufficiently high to prohibit equilibration of all three aryl hydrides with their η^2-arene counterparts at ambient temperature.

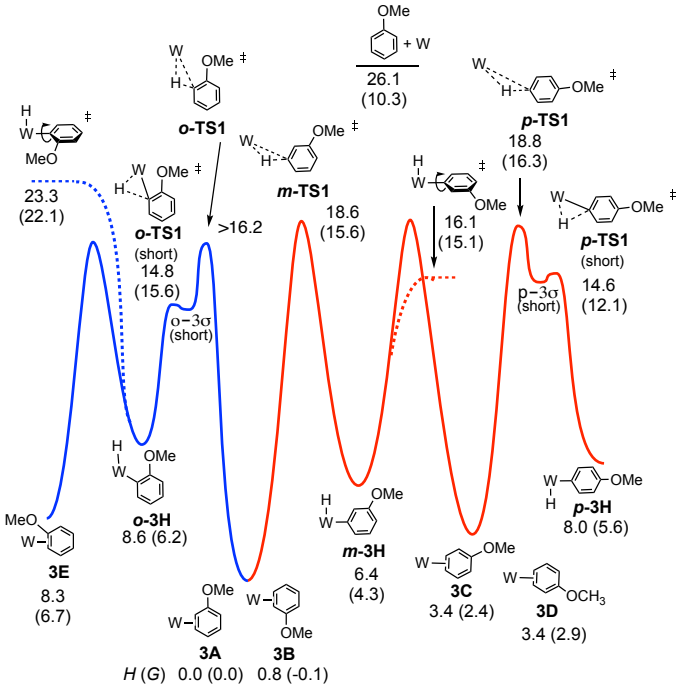

Figure 6. M06-calculated structures and abbreviated reaction coordinate profile for an interfacial for anisole complex isomers. W = {WTp(NO)(PMe$_3$)}; (kcal/mol). The energy of **o-TS1** is estimated to be greater than the energy of **o-3σ** (long) = 16.3 kcal/mol (not shown).

Interestingly, we found in the case of the anisole complex **3** that the ratio of **3** to **3H** can be modulated by choice of solvent. Table S10 in the SI summarizes these results, where we find that the use of MeOH enhances the amount of dihapto-coordinate arene at equilibrium to 23:1. We speculate that hydrogen bonding interactions with the basic NO ligand[45] could result in an overall decrease in electron density of the metal, and this could disfavor the formation of the oxidative addition process.

To study the effects of an electron-withdrawing substituent, we set out to prepare a complex of α,α,α-trifluorotoluene, using anisole complex **3** as a synthon for {WTp(NO)(PBu$_3$)}. Crystals of the trifluorotoluene complex (**4**) suitable for X-ray diffraction were prepared from a DCM/hexanes (1:10) solution of **4** at -30 °C. A molecular structure determination reveals that in the solid state *both* **4A** and **4B** are present. An ORTEP diagram of the higher population species (81:19) is provided in the SI.

^{1}H NMR analysis of the trifluorotoluene complex **4** reveals the presence of two η^2-arene complexes (**4A** (1.0) and **4B** (0.6)) along with two aryl hydrides (***m*-4H** (0.4) and ***p*-4H** (0.8)). The 1:0.6 ratio of **4A** and **4B** is comparable to that of the PMe$_3$ analog.[27] Interestingly, while exchanges on the timescale of the NOESY experiment were observed between the η^2-arene and aryl hydride complexes for **2** and **3**, no such exchange was observed for **4** at 25 °C. However, at 50 °C chemical exchange was observed between the para protons (H$_4$) of **4A** and **4B** and the hydride for ***p*-4H**. Also, exchange occurred between the two meta protons (H$_3$ and H$_5$) of **4A** and **4B** and the hydride of ***m*-4H** (Scheme 6). Given that the η^2-arene/aryl-hydride equilibrium constant is close to unity for all three arene systems **2** – **4**, the better π-accepting abilities of the electron-deficient CF$_3$Ph *appear to slow both the rate of oxidative addition and that of reductive elimination.* In other words, the CF$_3$ group not only stabilizes the η^2-arene isomer, making the transition state to the aryl hydride larger, but it also must stabilize the aryl hydride relative to this transition state, in order to keep the arene/aryl hydride equilibrium constant for **4** close to unity. Consistent with this idea, we calculated the energy effect of the CF$_3$ group on π coordination and stabilization of the aryl hydride. **4A** + benzene → **2** + trifluorotoluene ΔH = 4.1 kcal/mol and ΔG = 3.5 kcal/mol. Also, **4H** + benzene → **2H** + trifluorotoluene ΔH = 2.2 kcal/mol and ΔG = 1.9 kcal/mol. These calculated exchange reactions support the idea that both the η^2-arene and aryl hydride isomers are stabilized by the CF$_3$ group. Our calculations suggest that the origin of the slower isomerization is mainly this ground-state stabilization because ***o*-TS1-CF$_3$** + benzene → **TS1** + trifluorotoluene is exothermic and exergonic with ΔH = -0.4 kcal/mol and ΔG = -1.3 kcal/mol.

The spin transfer exchange observed with the trifluorotoluene system **4** is also consistent with an interfacial isomerization ("face-flip") mechanism operating through an aryl-hydride intermediate. In contrast, the previously reported MoTp(DMAP)(NO)(η^2-3,4-trifluorotoluene) complex (DMAP = 4-(dimethylamino)pyridine) is able to interconvert between the analogous coordination diastereomers predominantly through an intrafacial mechanism (ring-slip) that is operative at ambient temperatures.[46] We speculate that this difference in the predominant isomerization pathway between the Group 6 congeners is due to the more π-basic nature of the tungsten fragment. The further stabilization of the ground state for the tungsten system raises the barrier for the purported η^2-arene → sigma-complex transition state that is likely on the path to ring-walk (see Scheme 6). For both the molybdenum and rhenium systems mentioned above, any purported C-H insertion would likely result in a face-flip isomerization, which is not observed in the corresponding NOESY data.[41,46] Thus, C-H insertion is significantly slower than the ring-walk for both the Mo and Re complexes.

The temperature dependence of the C-H insertion process at the meta carbon was determined for a sample of **4** in acetonitrile-*d*$_3$ solution over a temperature range of 20 – 55 °C. A Van't Hoff plot (SI) shows that the reductive elimination (**m-4H** → **4**) is exothermic, with a $\Delta H°$ = -2.8 ± 0.2 kcal/mol and $\Delta S°$ = -9.0 ± 0.6 eu. These values are in good agreement with those obtained for the naphthyl hydride to naphthalene conversion on {RhCp*(PMe$_3$)} (cf. -4.1 kcal/mol, -12 eu),[22] as well as that calculated for **m-4H** to **4A** (-5.6 kcal/mol) and **2H** to **2** ($\Delta H°$ = -4.0 kcal/mol).

Scheme 6. Interfacial (face-flip) isomerization for the trifluorotoluene complex (**4A** to **4B**) involving two different aryl-hydride intermediates (***m*-4H**, ***p*-4H**); Values in parentheses are equilibrium ratios in benzene-d_6 at 25 °C.

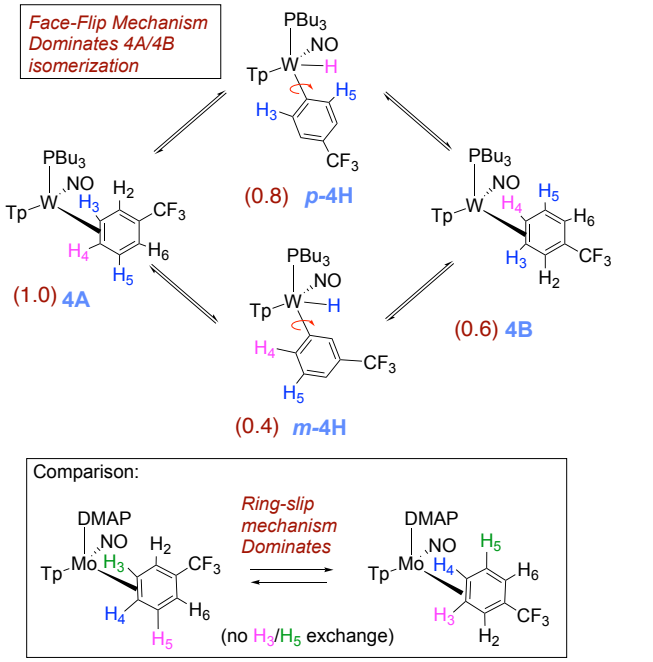

Beyond the complexes of benzene (**2**), anisole (**3**), and trifluorotoluene (**4**) already discussed, we surveyed *o*-hexafluoroxylene (**5**), pyridine-borane (**6**), naphthalene (**7**), thiophene (**8**), and cyclohexene (**9**). For the *o*-hexafluoroxylene benzene complex **5**, while initially no C-H activated product was observed, over five days in benzene-d_6 a new complex is formed in a 1:20 (**5H**:**5**) ratio that has resonances consistent with C-H activation (notably a new set of Tp4 protons at 5.76, 5.70 and 5.31 ppm) along with a resonance at 9.30 ppm with $J_{PH} = 98$ Hz and $J_{WP} = 31$ Hz) grows in over time. Analogous to **4**, the aryl hydride and η^2-arene forms of **5** do not undergo spin saturation exchange at ambient temperature and no fluctional behavior was observed even when heating the reaction mixture to 50 °C. Thus, *while substituents on the benzene ring have little impact on the arene/aryl-hydride equilibrium, they can have a major impact on the kinetics of C-H activation, ranging from seconds (benzene) to hours (o-hexafluoroxylene) at ambient temperatures.* For **7**-**9**, no C-H activated isomer was observed, even upon heating (50 °C) or over extended time (18 d).

We briefly explored different classes of aromatic molecules to determine to what extent the η^2-aromatic/aryl-hydride differed as a function of aromatic character of the ligand. For the pyridine-borane complex **6**, a 1.1:1 mixture of 3,4- and 4,5-η^2-pyridine isomers were identified in solution (Table 1),[47] along with a small amounts of two pyridinyl hydride isomers **6H** (5%; 9.40 ppm; $J_{PH} = 92.5$, $J_{WH} = 26.3$ Hz) and (**6H'**) (1%; 9.58 ppm; $J_{PH} = 96.0$ Hz). We tentatively assign these as C4- and C3-Aryl-hydrides, but the available data is insufficient to fully assign these species. For the π ligands in which η^2-complexation disrupts less of the inherent aromatic stability of the ligand,[5] the η^2-bound form is heavily favored. Such is the case with thiophene (**8**), naphthalene (**7**), and cyclohexene (**9**; Table 1). In these cases, we presume that an increased thermodynamic stability relative to the aryl or vinyl hydride is the reason for the lack of a hydridic species. For the latter complexes (**7**-**9**), ^{1}H NMR spectra closely match those of the PMe_3 analog, and characterization was not pursued further).[27, 48-49]

Table 1. Percentages of dihapto-coordinated aromatic complexes and their C-H insertion isomers at 25 °C. All values recorded in benzene-d_6 except for **5** recorded in acetone-d_6, and **9** in $CDCl_3$. Where equilibrium has been conclusively verified, this is noted.

η^2-Arene	(% of total)	Aryl Hydride	(% of total)
	46% (**2**)		54% (equilibrium)
	82% (**3**)	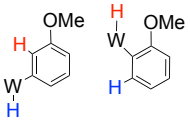	18% (equilibrium) 10 : 1
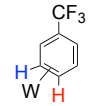	62% (**4**)	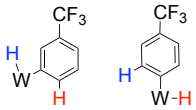	38% (equilibrium) 2 : 1
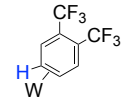	95% (**5**)	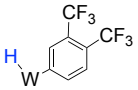	5% (equilibrium)
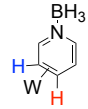	90% (**6**)	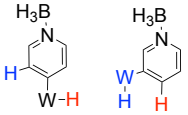	6% (equilibrium) 5 : 1[a]
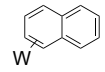	>99% (**7**)	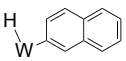	n.o.
	>99% (**8**)		n.o.
	>99% (**9**)		n.o.

a. assignment uncertain

As has been noted by Jones and co-workers for the rhodium-based systems RhCp(L) and RhCp*(L) (L = PMe_3, $P(OMe)_3$),[5] the equilibrium between η^2-arene and C-H activated adducts depends on the extent of disruption to the π-system when dihapto-coordination occurs. Hence just as for RhCp*(PMe_3), the [(η^2-R_2C=CHR)]/[(R_2C=CR)(H)] equilibrium ratio decreases as the ligand is adjusted from alkene to naphthalene to benzene. This trend is followed for the WTp(NO)(PBu_3) system. With regard to substituent effects, an interesting difference arises in the rhodium and tungsten systems. For RhCp*(PMe_3)(arene), the addition of a methoxy arene substituent shifts the η^2-naphthalene/naphthyl hydride

equilibrium to heavily favor the η^2-arene isomer.[21] In a similar manner, the addition of two CF_3 groups (*para*-hexafluoroxylene) shifts the benzene/phenyl hydride equilibrium to favor the η^2-arene.[50] In contrast, the introduction of either a OMe or CF_3 group to WTp(NO)(PMe_3)(benzene) leaves the equilibrium constant practically unchanged, despite clearly stabilizing the complex with respect to ligand dissociation in both cases (Table 2). Yet, as noted above, the *rate* of C-H activation dramatically decreases with the addition of one or two CF_3 groups.

For the rhodium system discussed above,[5] and as expected for oxidative addition in general,[51] the more electron-rich the metal, the more favorable oxidative addition is expected to be. It's tempting to attribute the increased amount of aryl hydride in equilibrium for **2** compared to its PMe_3 analog, to an increase in electron-donation from the PBu_3 ligand (cf. PMe_3). However, structural comparisons show negligible differences in metal-alkene bond lengths between **10** and the previously reported WTp(NO)(PMe_3)(η^2-cyclohexene) (SI). And, data collected from NMR and electrochemical experiments of the cyclohexene complex **10** closely resemble those of the analogous PMe_3 system(SI).[33] Further, while calculations indicate that ΔH for η^2-benzene $\rightarrow$ phenyl-hydride marginally increases (PMe_3 3.7 kcal/mol cf. PBu_3 2.4 kcal/mol; SI), the significant shift in the [η^2-arene]/[aryl hydride] ratio (from K =10 to K = 0.4; acetone, 0°C) resulting when PMe_3 is replaced by PBu_3 could also be attributed to the decrease in entropy experienced by the butyl chains in **2**, where their conformations have been restricted by the rigid η^2-bound benzene ring (Figure 7). Consistent with this notion, the methyl/butyl switch also causes the half-life to acetone substitution to be reduced from an hour to four minutes (acetone solvolysis) at 25 °C.

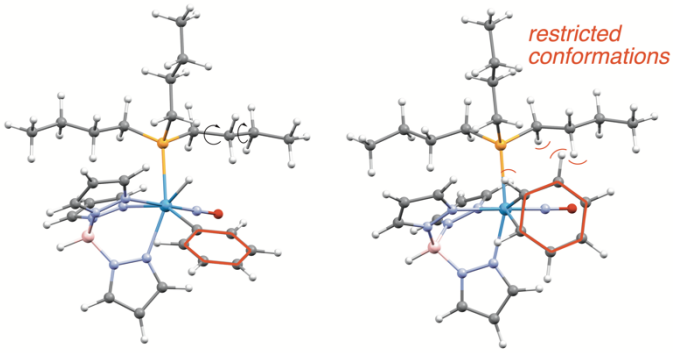

Figure 7. Comparison of the calculated structures for **2H** and **2** illustrating the restricted conformations of the butyl chains on **2** as a result of the protruding benzene ring.

Synthetic implications

Although roughly 40% of the trifluorotoluene complex **4** is in the form of an aryl hydride, we found that upon treatment with strong acid (HOTf in MeCN) a single η^2-arenium species (**10**) is formed. With spectroscopic features consistent with a distorted η^2-arenium intermediate.[33] Subsequent treatment with the masked enolate MTDA (MTDA = methyl trimethylsilyl dimethylketene acetal) yields the η^2-diene **11** prepared in situ (Scheme 7). This reactivity is fully consistent with that observed for the PMe_3 analog.[52] A single crystal XRD study of **11** (Figure 8) confirms the structure shown in Scheme 7. This complex (**11**) was subjected to oxidative decomplexation to provide the free organic methyl 2-methyl-2-(5-(trifluoromethyl)cyclohexa-2,4-dien-1-yl)propanoate (**12**) in 24% overall yield (The full characterization of this compound has been previously reported).[52] For comparison, the same series of transformations using the PMe_3 variant was accomplished with an overall yield of 32%. Compound **12** is a rare example of a diene with a CF_3 substituent. Such compounds are of interest in Diels-Alder reactions[42,43] and should be good candidates to participate in the inverse-electron-demand variant. As a practical note, in consideration of yields for all reactions starting from $W(CO)_6$, we estimate the cost to synthesize **12** starting from WTp(NO)(PBu_3)(Br) is roughly $1/4^{th}$ the cost in comparison to the published route from WTp(NO)(PMe_3)(Br).[52]

Scheme 7. Conversion of the trifluorotoluene complexes **4A**, **4B**, and **4H** to a functionalized cyclohexadiene **12**.

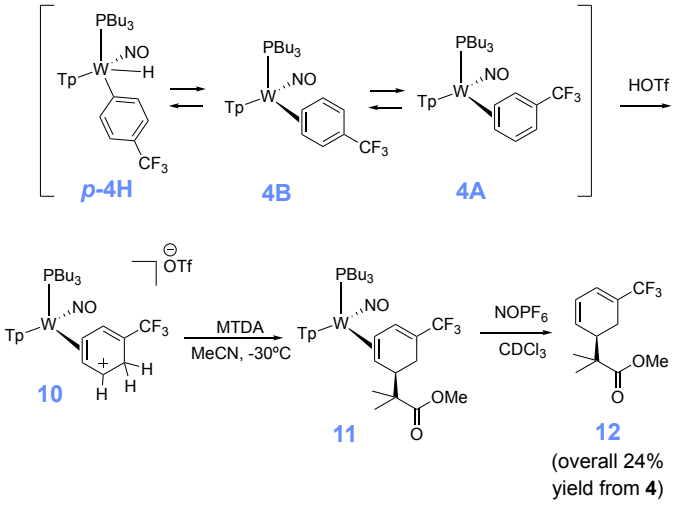

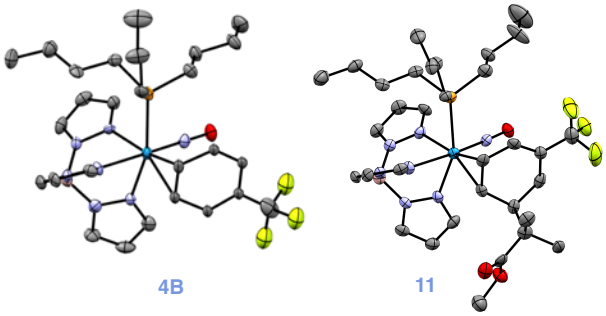

Figure 8. ORTEP diagrams (50% probablility) from SC-XRD studies of **4** and **11**. **4A** and **4B** co-crystalize, only **4B** (major isomer) is shown; hydrogens and solvent not included for clarity.

CONCLUSIONS

The complex WTp(NO)(PBu_3)(benzene) provides a rare example of an easily measurable equilibrium between an η^2-benzene complex and its phenyl hydride isomer, with an equilibrium constant close to unity at ambient temperatures. We have explored how temperature, solvent, and substituents on the benzene ring affect this equilibrium, and have carried out detailed DFT calculations that map out the pathways connecting these two ground states. *Whereas conventional wisdom says that a single lowest energy pathway connects a dihapto-coordinated benzene complex to its phenyl hydride isomer, passing through C-H sigma complex, our calculations reveal a network of intermediates and transition states connecting these two endpoints that are similar in energy, roughly 4 kcal/mol below dissociation, with no single pathway dominating.* We have also explored how these reaction pathways enable both interfacial (face-flip) and intrafacial (ring-slip) linkage isomerizations for the arene complex. Highlights of this study include:

1. Replacement of PMe_3 by PBu_3 creates an entropy penalty of roughly 2 kcal/mol at 298 K for the dihapto-coordinated isomer. This results in a significantly shorted substitution half-life ($\Delta G^{\ddagger}$ decreases), and a significant increase in the arene /phenyl-hydride equilibrium (ΔG decreases).
2. The bulkier phosphine does not appear to significantly increase the electron-density at the metal, as gauged by electrochemical potential, IR absorptions, and solid-state structural data.
3. The η^2-benzene and phenyl hydride isomers are connected through an intermediate best described as a C-H "sigma bond" complex. Two transition states (**TS1** and **TS2**) are closely associated with this intermediate and the energy surface for all three is remarkably flat. A third transition state (**TS3**) connects the η^2-benzene isomer to another benzene complex, still bound η^2, but held together primarily by dispersion forces.
4. Dynamics simulations reveal a complex network of pathways connecting oxidative addition, dihapto coordination, and arene dissociation. In particular, these calculations show that dihapto-coordination is not prerequisite for C-H activation.
5. In contrast to our previous findings with molybdenum, rhenium, and osmium η^2-benzene complexes, the tungsten systems undergo isomerization between the various η^2-arene isomers via a C-H insertion rather than via a ring slip.
6. The addition of either an OMe or a CF_3 substituent to the benzene ring increases the stability of *both* the η^2-arene and the aryl hydride isomers (with little change in the equilibrium constant). This is especially notable for the CF_3 analog, which for the dihapto-coordinate form has a substitution half-life over 250 times longer and a calculated bond strength that is five kcal/mol more stable than its benzene analog. The addition of a second CF_3 group further extends this trend.
7. When one or two CF_3 substituents are added to WTp(NO)(PBu_3)(benzene), the rate of C-H activation dramatically decreases from a half-life of seconds to hours without significantly impacting the η^2-arene/aryl-hydride equilibrium constant.
8. While there is an apparent correlation between the position of dihapto-binding and the C-H bond that is activated toward oxidative addition (see Table 2), this correlation is not causal. The observed regioselectivity of oxidative addition in this system appears to be governed strictly by thermodynamic factors.
9. Despite the presence of a considerable amount of aryl hydride, the novel organic chemistry of the η^2-trifluorotoluene ligand, initially reported for {WTp(NO)(PMe_3)}, is not compromised by replacement of PMe_3 with the bulkier phosphine, and the latter system is considerably more economical.

Returning to the larger subject of chemoselectivity of C-H functionalization, this study shows the role a substituent can play in determining not only location of C-H insertion (consider the high selectivity for meta insertion of anisole), but the rate of the insertion (with half-lives ranging from seconds to days). It also highlights the important role that temperature, solvent and the "outer sphere" of the ligand set (e.g., butyl groups) can play in influencing the complex equilibria existing between multiple η^2-arene and aryl hydride species.

EXPERIMENTAL SECTION

General Methods. NMR spectra were obtained on 500, 600 or 800 MHz spectrometers. Chemical shifts are referenced to tertramethylsilane (TMS) utilizing residual ^1H signals of the deuterated solvents as internal standards. Chemical shifts are reported in ppm and coupling constants (*J*) are reported in hertz (Hz). Chemical shifts for ^{19}F and ^{31}P spectra were reported relative to standards of hexafluorobenzene (164.9 ppm) and triphenylphosphine (-6.00 ppm). Infrared Spectra (IR) were recorded on a spectrometer as a solid with an ATR crystal accessory, and peaks are reported in cm^{-1}. Electrochemical experiments were performed under a nitrogen atmosphere. Most cyclic voltammetric data were recorded at ambient temperature at 100 mV/s, unless otherwise noted, with a standard three electrode cell from +1.8 V to -1.8 V with a platinum working electrode,

acetonitrile (MeCN) solvent, and tetrabutylammonium (TBAH) electrolyte (~1.0 M). All potentials are reported versus the normal hydrogen electrode (NHE) using cobaltocenium hexafluorophosphate ($E_{1/2}$ = -0.78 V, -1.75 V) or ferrocene ($E_{1/2}$ = 0.55 V) as an internal standard. Peak separation of all reversible couples was less than 100 mV. All synthetic reactions were performed in a glovebox under a dry nitrogen atmosphere unless otherwise noted. All solvents were purged with nitrogen prior to use. Deuterated solvents were used as received from Cambridge Isotopes and were purged with nitrogen under an inert atmosphere. When possible, pyrazole (Pz) protons of the (trispyrazolyl) borate (Tp) ligand were uniquely assigned (e.g., "Tp3B") using two-dimensional NMR data (see Fig. S1). If unambiguous assignments were not possible, Tp protons were labeled as "Tp3/5 or Tp4". All *J* values for Tp protons are 2 (±0.4) Hz.

Synthesis of WTp(NO)(PBu$_3$)(Br) (1)

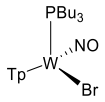

A 100 mL round bottom flask was charged with WTp(Br)$_2$(NO) (18.48 g, 31.6 mmol) along with 80 mL of DCM that had been purged with $N_{2(g)}$ and the heterogeneous yellow reaction mixture was allowed to vigorously stir. Zn dust (7.05 g, 100.8 mmol) was added to this mixture followed *immediately* by the addition of tri(n-butyl)phosphine (10.03 g, 49.6 mmol). Initially the reaction mixture turned to a lime green color. The solution was allowed to sit for 40 min at which point the reaction mixture had turned to a deep green color. The reaction mixture was then loaded onto a medium 150 mL fritted disc that had been filled with two inches of neutral alumina and covered in DCM. The green reaction mixture was then eluted through the neutral alumina column and a vibrant dark green band was eluted with DCM (200 mL) into a 500 mL filter flask. The DCM solvent was then concentrated *in vacuo* until ~ 100 mL solvent remained. To this homogeneous green solution was added 200 mL hexanes until a green precipitate was observed to form in solution. Filtering the heterogeneous green reaction mixture through a fine 60 mL fritted disk allowed for the recovery of a deep green crystalline solid. This solid was then washed 3 x 20 mL pentane and allowed to dry under dynamic vacuum in a desiccator for six hours before a mass was taken (9.16 g, 42%). The paramagnetic nature of the compound prevented use of NMR spectroscopy, but crystals of **1** of suitable quality for X-ray diffraction were grown utilizing vapor diffusion by dissolving in DCM and allowing ether to diffuse into the mixture over several days.

CV (MeCN) $E_{1/2}$ = -1.36 V, $E_{p,a}$ = 0.44 V (NHE). IR: ν(BH) = 2521 cm^{-1}, ν(NO) = 1580 cm^{-1}.
Anal. Calcd for $C_{21}H_{37}BBrN_7OPW$: C, 35.57; H, 5.26; N, 13.87. Found: C, 35.67; H, 5.26; N, 13.99.

Synthesis of WTp(NO)(PBu$_3$)(η^2-benzene) (2) and WTp(NO)(PBu$_3$)(H)(C$_6$H$_5$) (2H)

A 250 mL oven dried round bottom flask was loaded with **1** (6.02 g, 8.50 mmol) followed by benzene (200mL) and the homogeneous green reaction mixture was allowed to stir. To this solution was added 30-33% by weight sodium dispersion in paraffin (7.04 g, 54.0 mmol). After 4 h of stirring the reaction mixture had turned to a golden yellow color and completion of the reaction was confirmed by cyclic voltammetry (no indication of **1**). The golden-brown reaction mixture was then filtered through a coarse 60 mL fritted disc that had been filled with one inch of Celite and set in pentane. The Celite was then washed with 100 mL of ether to collect a brown band that developed on the Celite. This reaction mixture was then loaded on a coarse 150 mL fritted disc that had been filled with two inches of silica and saturated with pentane. A yellow band was then eluted with a 10:1 ether:benzene mixture (300 mL total), collected, and then concentrated until 50 mL of solution remained. To this solution was added 200 mL of pentane. The volume was reduced by half *in vacuo* until a yellow solid precipitated from solution. The mixture was then filtered through a fine 30 mL fritted disc to isolate a vibrant yellow solid. This solid was then washed with chilled pentane (3 x 10 mL) and allowed to desiccate for six hours to yield a bright yellow powder (1.21 g, 20%).

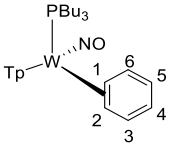

2

CV (MeCN) $E_{p,a}$ = -0.16 V (NHE). IR: ν(BH) = 2504 cm^{-1}, ν(NO) = 1564 cm^{-1}. ^{1}H-NMR (acetone-d_6, δ, 0 °C): 8.00 (1H, d, Tp5), 7.99 (1H, d, Tp5), 7.94 (1H, d, Tp3), 7.85 (1H, d, Tp5), 7.45 (1H, d, Tp3C), 6.97 (1H, d, Tp3A), 6.81 (1H, buried, H6), 6.80 (1H, buried, H3), 6.36 (1H, t, Tp4), 6.30 (2H, overlapping t, Tp4), 5.70 (2H, overlapping m, H4 and H5), 4.11 (1H, m, H1), 2.30 (1H, m, H2), 1.26 (6H, m, PBu$_3$), 1.14 (6H, overlapping with **2H**, PBu$_3$), 0.89 (6H, overlapping with **2H**, PBu$_3$), 0.76 (9H, t, J = 7.3, PBu$_3$). ^{31}P-NMR (benzene-d_6, δ, 25°C): -2.74 (J_{WP} = 308).^{13}C-NMR (acetone-d_6, δ, 0°C): 141.9 (Tp3/5), 141.3 (Tp3/5), 137.4 (Tp3/5), 136.6 (Tp3/5), 136.1 (Tp3/5), 134.4 (Tp3/5), 133.2 (C6), 128.9 (C3), 117.4 (C4/C5), 116.6 (C4/C5), 107.0 (Tp4), 106.9 (Tp4), 106.1 (Tp4), 63.9 (C2), 62.9 (C1, J_{PC} = 8.6), 26.6, 26.0, 25.5, 25.1, 24.9, 22.6, 14.4 14.1 (overlapping PBu$_3$ signals for **2** and **2H isomer**).

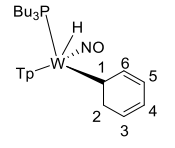

2H

IR: ν(WH) = 1989 cm^{-1}. ^{1}H-NMR (acetone-d_6, δ, 0 °C): 9.62 (1H, m, J_{WP} = 97.3, J_{WH} = 31.1 ,W-H), 8.15 (1H, d, Tp3/5), 8.06 (1H, d, Tp3/5), 8.04 (1H, d, Tp3/5), 7.75 (1H, d, Tp3/5), 7.68 (1H, d, Tp3/5), 7.20 (2H, broad, H2 and H6), 6.97 (1H, d, Tp3/5), 7.20 (2H, broad, H3/H5), 6.81 (2H, t, J = 7.2, H2/6), 6.71 (1H, t, J = 7.2, H4), 6.45 (1H, t, Tp4), 6.41 (1H, t, Tp4), 5.94 (1H, t, Tp4), 1.26, 1.14, 0.89 (overlapping PBu$_3$ resonances for **2** and **2H isomers**), 0.79 (9H, t, J = 7.3, PBu$_3$). ^{31}P-NMR (benzene-d_6, δ, 25°C): +16.3 (J_{WP} = 173). ^{13}C-NMR (acetone-d_6, δ, 0 °C): 178.5 (C1, J_{PC} = 6.0), 145.9 (Tp3/5), 145.7 (Tp3/5), 145.2 (Tp3/5), 138.3 (Tp3/5), 137.4 (Tp3/5), 137.3 (Tp3/5), 135.4 (C2/C6), 127.6 (C3/C5), 107.3 (Tp4), 107.0 (Tp4), 105.7 (Tp4), 26.6, 26.0, 25.5, 25.1, 24.9, 22.6, 14.4 14.1 (overlapping PBu$_3$ signals for **2** and **2H isomers**).

Synthesis of WTp(NO)(PBu$_3$)(η^2-2,3-anisole) (3A and 3B) and WTp(NO)(PBu$_3$)(H)(C$_6$H$_4$OMe) (o-3H and m-3H)

An oven-dried 250 mL round bottom flask was charged with a stir bar and 200 mL of anisole, followed by complex **1** (11.35g, 16.0 mmol) and allowed to vigorously stir to generate a homogeneous green reaction mixture. Next 30-33% by weight sodium dispersion in paraffin (6.13 g, 88.8 mmol) was added. After 2.5 h, the reaction mixture had turned to a golden yellow color and the reaction was confirmed to be completed by cyclic voltammetry after a ~2 mL aliquot of this reaction mixture had been filtered through a pipette-column filled with Celite.

The bulk golden-brown reaction mixture was then filtered through a coarse 150 mL fritted disc that had been filled with two inches of Celite and saturated with anisole. Vacuum was applied to elute the colored filtrate and the Celite plug was washed with 100 mL of addition anisole to collect the brown solution into a 500 mL filter flask. The filtrate was then loaded onto a 10 cm silica column on a coarse 150 mL fritted disc that had been set in pentane. After the entire filtrate had been loaded the column was washed with 250 mL pentane total to wash away free anisole. The column was then rinsed with ~200 mL of ether to elute a vibrant orange band. Once the orange band was near the bottom of the column, the clear filtrate was discarded and elution with ether continued so as to collect the desired product. The orange band on the column was eluted with a total of 700 mL and collected in a 1000 mL filter flask. In the filter flask the initially orange band now appears as a homogeneous yellow solution. The solvent was the removed in vacuo until the volume had been reduced to < 100 mL of ether. To this solution was added 500 mL of pentane to generate a heterogeneous yellow mixture. The volume was reduced by half in vacuo and the resulting yellow solid was filtered through a fine 60 mL fritted disc and wash with 3 x 30 mL pentane to yield a vibrant yellow solid (5.79g, 49 %). Single-crystals suitable for X-ray diffraction were grown from a DCM/pentane mixture that was allowed to sit at -30 °C over several hours to grow **3A** and support the elemental composition of the complex.

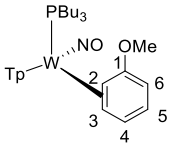

3A

CV (MeCN) $E_{p,a}$ = -0.17 V (NHE). IR: ν(BH) = 2488 cm^{-1}, ν(NO) = 1559 cm^{-1}. ^{1}H-NMR (acetone-d_6, δ, 0 °C): 8.13 (1H, d, Tp3A), 8.00 (1H, d, Tp3/5), 7.97 (1H, d, Tp3/5B), 7.95 (1H, d, Tp5C), 7.84 (1H, d, Tp5A), 7.41 (1H, d, Tp3C), 6.41 (1H, overlap, H4), 6.35 (1H, t, Tp4B), 6.31 (1H, t, Tp4C), 6.27 (1H, t, Tp4A), 5.70 (1H, dd, J = 6.9, 1.7, H5), 5.08 (1H, d, J= 6.9, H6) 4.01 (1H, t, J = 10.7, H2), 3.68 (3H, s, OMe), 2.30 (1H, m, H3), 2.20, 2.03, 1.93, 1.86, 1.75, 1.27, 1.14, 1.00, 0.88,0.78 (overlapping PBu_3 resonances for **3A, 3B, m-3H**). ^{31}P-NMR (DME, δ, 25°C): -3.34 (J_{WP} = 303).^{13}C-NMR (acetone-d_6, δ, 0 °C): 165.1 (C1), 145.7 (Tp3/5), 141.9 (Tp3/5), 141.5 (Tp3/5), 137.3 (Tp3/5), 136.7 (Tp3/5), 136.2 (Tp3/5), 124.8 (C4), 117.2 (C5), 107.0 (Tp4), 106.8 (Tp4), 105.9 (Tp4), 91.6 (C6), 64.5 (C3), 58.4 (C2, d, J_{PC} = 10.9), 54.0 (OMe), 26.5, 26.0, 25.4, 25.1, 24.9, 22.9, 22.6, 14.0 (overlapping PBu_3 resonances for **3A, 3B, m-3H**).

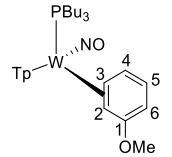

3B

^{1}H-NMR (acetone-d_6, δ, 0 °C): 8.13 (1H, d, Tp3A), 8.05 (1H, d,Tp3B/C), 7.99 (1H, d, Tp3/5), (1H, d, Tp3/5), 7.45 (1H, d, Tp3/5), 7.05 (1H, d, Tp3/5), 7.46(1H, d, Tp3C), 6.34 (1H, t, Tp4C), 6.30 (2H, overlapping resonances for **3A, 3B, m-3H**, Tp4A/B and H4), 5.60 (1H, dd, J = 6.5, 2.1, H5), 4.89 (1H, d, J = 6.5, H6), 4.18 (1H, m, H3), 2.30 (1H, m, H2), 2.20, 2.03, 1.93, 1.86, 1.75, 1.27, 1.14, 1.00, 0.88, 0.78 (overlapping PBu_3 resonances for **3A, 3B, m-3H**).^{31}P-NMR (DME, δ, 25°C): -2.98 (J_{WP} = 299). ^{13}C-NMR (acetone-d_6, δ, 0 °C): 159.7 (C1), 135.0-147.0 overlapping Tp3/5 resonances for **3A, 3B, m-3H**, 141.8 (Tp3/5), 145.8 (Tp3/5), 107.6 (Tp4), 106.5 (Tp4), 105.0 (Tp4). 125.0 (C4), 117.2 (C5 overlap with **3A**), 88.8 (C6), 63.1 (C3, d, J_{PC} = 11.1), 60.6 (C2), 53.9 (OMe), 26.5, 26.0, 25.4, 25.1, 24.9, 22.9, 22.6, 14.0 (overlapping PBu3 resonances for **3A, 3B, m-3H**).

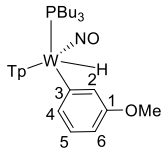

m-3H

^{1}H-NMR (acetone-d_6, δ, 0 °C): 9.57 (1H, m, J_{PH} = 97.2, J_{WH} = 31.2, W-H), 8.03 (1H, d,Tp3/5), 7.85 (1H, d,Tp3/5), 7.77 (1H, d,Tp3/5), 7.45 (1H, d,Tp3/5), 7.68 (1H, d,Tp3/5), 7.28 (1H, t, J = 8.05, H5), 7.05 (1H, d,Tp3/5), 6.92 (1H, s, H4), 6.76 (1H, broad, H6), 6.44 (1H, t, Tp4), 6.30 (2H, buried, H2 and Tp4), 5.95(1H, t, Tp4), 3.51 (3H, broad s, OMe). 2.20, 2.03, 1.93, 1.86, 1.75, 1.27, 1.14, 1.00, 0.88, 0.78 (overlapping PBu_3 resonances for **3A, 3B, m-3H**).^{31}P-NMR (DME, δ, 25°C): 15.55 (J_{WP} = 176).^{13}C-NMR (acetone-d_6, δ, 0 °C): 180.1 (C3), 159.7 (C1), 144.3(Tp3/5), 142.9 (Tp3/5), 136.5 (Tp3/5), 135.2 (Tp3/5), 134.5 (Tp3/5), 130.9 (C4), 127.7 (C6), 125.0 (C2), 121.0 (C4), 107.3 (Tp4), 105.7 (Tp4), 106.4 (Tp4), 53.9 (OMe), 26.5, 26.0, 25.4, 25.1, 24.9, 22.9, 22.6, 14.0 (overlapping PBu_3 resonances for **3A, 3B, m-3H**).

Synthesis of WTp(NO)(PBu_3)(η^2-3,4-a,a,a-trifluorotoluene) (4A and 4B) and WTp(NO)(PBu_3)(H)($C_6H_5CF_3$) (p-4H and m-4H)

A 4-dram vial was charged with a stir pea, trifluorotoluene (2 mL, 16.2 mmol) and **2** (1.00 g, 1.35 mmol) and the initially homogeneous yellow reaction mixture was allowed to stir. Over time the reaction mixture turns from a homogeneous yellow to a heterogeneous yellow and at the end of 6 h this reaction mixture was added to 10 mL of pentane and allowed to sit at -30 °C for 30 min. The heterogeneous yellow mixture was then filtered through a fine 15 mL fritted disc to yield a vibrant yellow-gold powder. This powder was washed with 3 x 10 mL of pentane that had been chilled to -30 °C and allowed to dry under active vacuum in a desiccator for 4 h and then static vacuum in a desiccator overnight. A mass was then taken the next day of the product, a vibrant yellow solid (0.716 g, 68 %).

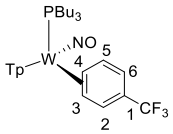

4B

CV (MeCN) $E_{p,a}$ = +0.10 V (NHE). IR: ν(BH) = 2519 cm^{-1}, ν(NO) = 1567 cm^{-1}. ^{1}H-NMR (MeCN-d_3, δ, 0 °C): 7.93 (1H, d, Tp3/5), 7.88-7.90 (4H, overlapping Tpd resonances with **4A, 4B, p-4H and m-4H**), 7.80 (2H, overlapping d, Tp3/5), 7.33 (1H, d, J= 5.9, H2), 6.97 (2H, overlapping, H5), 6.33 (1H,t, overlapping resonances with **4A, 4B, p-4H and m-4H**, Tp4), 6.31 (1H, t, Tp4), 6.25 (1H, t overlapping resonances with **4A, 4B, m-4H and p-4H**, Tp4), 5.76 (1H, overlapping d, H6), 3.89 (1H, m, H4), 2.08 (1H, m, H3), 1.83 (6H, overlapping resonances with **4A, 4B, p-4H and m-4H**, PBu_3), 1.24 (6H, overlapping resonances with **4A, 4B, p-4H and m-4H**, PBu_3), 1.08 (6H, overlapping resonances with **4A, 4B, p-4H and m-4H** PBu_3), 0.80 (9H, overlapping resonances with **4A, 4B, p-4H and m-4H**, PBu_3). ^{31}P-NMR (MeCN-d_3, δ, 25°C): -4.77 (J_{WP} = 294).^{19}F-NMR (MeCN-d_3, δ, 25°C): -62.88 (CF_3, s).^{13}C-NMR (MeCN-d_3, δ, 0°C): 146.0 (3C, overlapping resonances with **4A, 4B, p-4H and m-4H**, Tp3/5), (3C,

141.9, overlapping resonances with **4A, 4B, p-4H and m-4H**, Tp3/5), 111.1 (C1 of **4B**), 106.2 to 107.7 (Tp4, overlapping resonances with **4A, 4B, p-4H and m-4H**), 126.0 or 125.3 (CF_3, q, J_{CF} = 269.0 or 267.0), 63.2 (C4, d, J_{PC} = 9.2), 63.5 (C3), 25.3 (overlapping PBu3 resonances), 25.0 (overlapping PBu_3 resonances with **4A, 4B, p-4H and m-4H**), 22.8 (overlapping PBu_3 resonances for isomers **4A, 4B, p-4H and m-4H**), 13.9 (overlapping PBu_3 resonances with **4A, 4B, p-4H and m-4H**). Anal. Calcd for $C_{28}H_{42}BF_3N_7OPW$: C, 43.38; H, 5.46; N, 12.65. Found: C, 43.08; H, 5.52; N, 12.39..

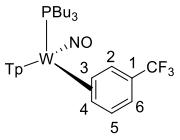

4A

^{1}H-NMR (MeCN-d_3, δ, 0 °C): 8.07 (1H, d, Tp3A), 7.90 (3H, overlapping d, Tp3/5), 7.79 (1H, d, Tp5A), 7.38 (1H, d, 5.13, H2), 7.29 (1H, d, Tp3C), 6.97 (1H, overlapping, H5), 6.33 (1H, t, Tp4B), 6.29 (1H, t, Tp4A), 6.25 (1H, t, Tp4C), 5.76 (1H, overlapping, H6), 3.76 (1H, m, H3), 2.17 (1H, m, H4), 1.83 (6H, overlapping with other isomers **4A, 4B, p-4H and m-4H**, PBu_3), 1.24 (6H, overlapping with other isomers **4A, 4B, p-4H and m-4H**, PBu_3), 1.08 (6H, overlapping with other isomers **4A, 4B, p-4H and m-4H**, PBu_3), 0.80 (9H, overlapping with other isomers **4A, 4B, p-4H and m-4H**, PBu_3). ^{31}P-NMR (MeCN-d_3, δ, 25°C): -5.09 (J_{WP} = 294).^{19}F-NMR (MeCN-d_3, δ, 25°C): -62.13 (CF_3, s). ^{13}C-NMR (MeCN-d_3, δ, 0 °C): 146.0 (3C, overlapping with other isomers Tp3/5), (3C, 141.9 overlapping with other isomers), 135.7 (overlapping C2 and C5), 110.3 (C6), 126.0 or 125.3 (CF_3, q, J_{CF} = 269 or 267), 106.2 to 107.7 (overlapping Tp4 resonances for isomers **4A, 4B, p-4H and m-4H**), 63.6 (C4), 60.3 (C3, d, J_{PC} = 7.9), 25.3 (overlapping PBu_3 resonances for isomers **4A, 4B, p-4H and m-4H**), 25.0 (overlapping PBu_3 resonances for isomers **4A, 4B, p-4H and m-4H**), 22.8 (overlapping PBu_3 resonances for isomers **4A, 4B, p-4H and m-4H**), 13.9 (overlapping PBu_3 resonances for isomers **4A, 4B, p-4H and m-4H**).

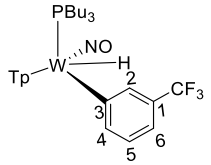

m-4H

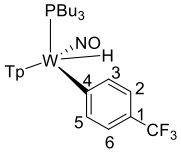

p-4H

Select resonances for **m-4H and p-4H**

^{1}H-NMR (MeCN-d_3, δ, 0 °C): 9.59 (1H, m, J_{PH} = 98, J_{WP} = 30,W-H for **p-4H**), 9.56 (1H, m, J_{PH} = 95, J_{WP} = 30, W-H for **m-4H**), 7.64 (1H, d, overlapping Tpd for either **p-4H** or **m-4H**), 7.11 (1H, d, J = 7.19, Ph-Ring proton for **p-4H** or **m-4H**), 7.06 (1H, d, J = 7.44, Ph-Ring proton for **p-4H** or **m-4H**), 6.91 (3H, buried, overlapping Tpd for either **p-4H** or **m-4H** and H3/5 for **p-4H**), 5.95 (1H, t, Tp4 for **m-4H**), 5.94 (1H, t, Tp4 for **p-4H**). ^{31}P-NMR (MeCN-d_3, δ, 25°C): 15.80 and 15.53, (J_{WP} = 176 for 15.53 resonance, J_{WP} = 174 for 15.80 resonance, **p-4H** and **m-4H**).^{13}C-NMR (MeCN-d_3, δ, 0 °C): 180.2 (overlapping C4 and C3 for **p-4H** and **m-4H**), 146.1 (Ph-ring carbon for **p-4H**), 145.0 (Ph-ring-carbon for **m-4H**), 136.3 (Ph-ring carbon for **p-4H**), 130.5 (Ph-ring carbon for **p-4H**).

Synthesis of WTp(NO)(PBu_3)(η^2-4,5,-bis-trifluoromethylbenzene) (5)

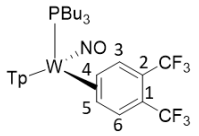

A 4-dram vial was charged with a stir bar, 1,2-bis(trifluoromethyl)benzene (2.00 g, 9.34 mmol) and **3** (0.103 g, 0.140 mmol) and the initially homogeneous yellow reaction mixture was allowed to stir for 24 h. Over time the reaction mixture turns from a homogeneous yellow to a light brown color and at the end of 6 h this reaction mixture was added to 10 mL of pentane and allowed to sit at -30 °C for 16 h. Over time crystals suitable for x-ray diffraction developed and the light tan solid was then isolated on a fine 15 mL fritted disc. This solid was then washed with 3 x 10 mL of pentane that had been chilled to -30 °C and allowed to dry under static vacuum for 16 h. A mass was then taken the next day of the product, a light tan solid (0.053 g, 45 %). Atomic composition consistent with crystal structure.

CV (MeCN) $E_{p,a}$ = +0.47 V (NHE). IR: ν(BH) = 2490 cm^{-1}, ν(NO) = 1587 cm^{-1}. ^{1}H-NMR (benzene-d_6, δ, 25 °C): 8.18 (1H, d, Tp3/5), 7.80 (1H, d, J= 6.50, H6), 7.79 (1H, d, Tp3/5), 7.71 (1H, d, J= 5.9, H3), 7.30 (1H, d, Tp3/5), 7.28 (1H, d, Tp3/5), 7.26 (1H, d, Tp3/5), 6.71 (1H, d, Tp3/5), 5.75 (2H, overlapping t, Tp4), 5.69 (1H, t, Tp4), 3.42 (1H, m, H4), 2.12 (1H, m, H5), 1.71 (3H, m, PBu_3), 1.59 (3H, m, PBu_3), 1.15 (3H, m, PBu_3), 1.10 (3H, m, PBu_3), 0.91 (3H, m, PBu_3), 0.78 (9H, t, J= 7.36, PBu_3),^{31}P-NMR (benzene-d_6, δ, 25°C): -3.96 (J_{WP} = 292).^{19}F-NMR (benzene-$d6$, δ, 25°C): -57.6 (3F, q, J_{FF} = 12.6, CF_3), -57.9 (3F, q, J_{FF} = 12.6, CF_3). ^{13}C-NMR (benzene-d_6, δ, 25 °C): 145.6 (Tp3/5), 142.3 (Tp3/5), 140.7 (Tp3/5), 140.4 (C6, q, J_{CF} = 7.2), 139.3 (broad, C3), 136.4 (Tp3/5), 135.8 (Tp3/5), 135.5 (Tp3/5), 125.1 (overlapping CF_3 resonances, J_{CF} = 270.0), 115.1 (q, J_{CF} = 31.1, C1/C2), 113.2 (q, J_{CF} = 31.1, C1/C2), 106.6 (Tp4), 106.5 (Tp4), 106.4 (Tp4), 60.1 (C5), 60.0 (C4, J_{PC} = 9.3), 25.1 (d, J_{PC} = 3.1, PBu_3), 24.7 (d, J_{PC} = 12.4, PBu_3), 22.8 (d, J_{PC} = 23.1, PBu_3), 13.8 (PBu_3).

Synthesis of WTp(NO)(PBu_3)(η^2-3,4-pyridineborane) (6)

A solid of **3** (500 mg, 0.678 mmol) was added to a 4-dram vial containing stirring neat pyridine-borane (3.00 g, 32.3mmol). After stirring for 2 h, the reaction mixture was diluted with 6 mL THF, followed by 25 mL Et_2O and then 90 mL of hexanes. The solution was allowed to settle for 15 min, while a Celite column (1 cm tall) was prepared in a 15 mL medium porosity fritted disk. The solution was decanted through the Celite, leaving a green oil. The oil was again diluted with 6 mL THF, followed by 25 mL Et_2O and then 90 mL of hexanes. The solution was decanted through the Celite, leaving a clumpy material in the vial. The material captured by the Celite was dissolved in 6 mL THF and returned to the vial. Upon complete dissolution of all solids, the solution was diluted with 25 mL followed by 150 mL hexanes. The precipitate was collected on the Celite column, and then redissolved with 20 mL THF. The resulting solution was diluted with 35 mL Et_2O and 150 mL hexanes, forming a bright yellow precipitate. The precipitate was collected on a 15 mL medium porosity fritted funnel, rinsed with 2 x 5 mL hexanes, transferred wet to a vial, and placed under dynamic vacuum (0.185 g, 38%).

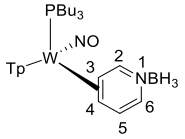

CV (DMA) $E_{p,a}$ = +0.59 V (NHE). IR: ν(BH) = 2519 cm^{-1}, ν(BH$_3$) = 2348, 2288, 2256 cm^{-1}, ν(NO) = 1587 cm^{-1}. ^{1}H-NMR (acetone-d_6, δ, 15 °C): 8.62 (1H, d, J = 4.21, H2), 8.14 (1H, d, Tp3/5), 8.09 (1H, Tp3/5), 8.04 (1H, d,Tp3/5), 7.92 (2H, d overlapping, Tp3/5), 7.62 (1H, d, Tp3/5), 6.77 (1H, t, J= 6.34, H5), 6.44 (1H, t, Tp4), 6.37 (1H, t, Tp4), 6.34 (1H, t, Tp4), 6.18 (1H, d, J = 7.03, H6), 3.65 (1H, m, H3), 2.17 (1H, t, J = 7.54, H4), 1.92 (6H, m overlapping with minor, PBu3), 1.20 (12H, overlapping resonances and overlapping with minor, PBu$_3$), 0.79 (9H, t, J = 7.51, PBu$_3$). ^{31}P-NMR (acetone-d_6, δ, 25 °C): -3.6 (PMe$_3$, J_{WP} = 284). ^{13}C-NMR (acetone-d_6, δ, 0 °C): 167.7 (C2), 146.0 (Tp3/5), 142.3 (Tp3/5), 141.7 (Tp3/5), 138.2 (Tp3/5), 137.4 (Tp3/5), 136.7 (Tp3/5), 127.2 (C5/6), 125.3 (C5/6), 107.6 (Tp4 overlapping with minor), 107.4 (Tp4), 106.7 (Tp4), 61.1 (C4), 59.3 (C3, d, J_{PC} = 7.1), 25.5 (PBu$_3$ overlap with minor isomer), 25.0 (PBu$_3$, overlap with minor isomer **6B**), 23.4 (PBu$_3$, d, J_{PC} = 24.6), 14.0 (PBu$_3$ overlap with minor isomer **6A**). Anal. Calcd for $C_{26}H_{45}B_2N_8OPW$: C, 43.24; H, 6.28; N, 15.52. Found: C, 42.94; H, 6.31; N, 15.37.

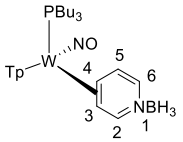

^{1}H-NMR (acetone-d_6, δ, 15 °C): 8.50 (1H, d, J= 4.50, H2), 8.10 (1H, d, Tp3/5), 8.09 (2H, d overlapping, Tp3/5), 8.01 (1H, d,Tp3/5), 7.92 (1H, d overlapping with major, Tp3/5), 7.59 (1H, d, Tp3/5), 6.74 (1H, t, J = 6.62, H5), 6.43 (1H, t, Tp4), 6.41 (1H, t, Tp4), 6.39 (1H, t, Tp4), 6.24 (1H, d, J = 6.62, H6), 3.92 (1H, m, H4), 2.07 (1H, buried, H3), 1.91 (6H, m overlapping with major, PBu$_3$), 1.20 (12H, overlapping resonances and overlapping with major, PBu$_3$), 0.77 (9H, t, J = 7.41, PBu$_3$). ^{31}P-NMR (acetone-d_6, δ, 25 °C): -3.9 (J_{WP} = 291). ^{13}C-NMR (acetone-d_6, δ, 0 °C): 169.9 (C2), 146.4 (Tp3/5), 144.1 (Tp3/5), 142.3 (Tp3/5), 138.1 (Tp3/5), 137.6 (Tp3/5), 136.7 (Tp3/5), 127.6 (C5/6), 126.7 (C5/6), 107.6 (Tp4 overlapping with minor), 107.5 (Tp4), 107.1 (Tp4), 61.4 (C4, d, J_{PC} = 9.86), 58.8 (C3), 25.5 (PBu$_3$ overlap with major isomer), 25.0 (PBu$_3$, overlap with major isomer), 22.8 (PBu$_3$, d, J_{PC} = 24.2), 14.0 (PBu$_3$ overlap with major isomer).

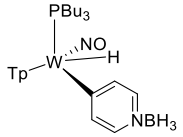

Partial HNMR data of **6H** (5%): ^{1}H-NMR (acetone-d_6, δ, 25 °C): 9.40 (1H, m, J_{PH} = 92.5, J_{WH} = 26.3, W-H), 8.20 (1H, d, Tp3/5), 8.08 (1H, Tp3/5), 7.80 (1H, d,Tp3/5), 7.79 (1H, d, Tp3/5), 7.14 (1H, d, Tp3/5), 6.53 (1H, t, Tp4), 6.14 (1H, t, Tp4). **6H'** (1%): 9.58 ppm with a J_{PH} = 96.0 Hz (not enough signal to determine J_{WH}).

Synthesis of WTp(NO)(PBu$_3$)(η^2-1,2-cyclohexene) (9)

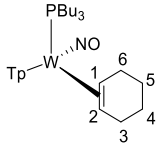

To a 4-dram vial was added **3** (0.492 g, 0.67 mmol) along with cyclohexene (1 mL, 9.9 mmol). The initially heterogeneous yellow reaction mix was allowed to stir over 4 h, during which time the solution turned to a light homogeneous brown color. The reaction mixture was then added to 15 mL of pentane that had been chilled to -30 °C to precipitate out a light pink solid. This solid was then collected on a fine 15 mL fritted disc. The solid was then washed with 3 x 5 mL pentane and the filtrate was evaporated in vacuo and subseuqently picked up in a minimal amount of DCM (1 mL) and added to 15 mL of standing pentane ina 4-dram vial. This solution was allowed to sit at -30 °C overnight during which time a light yellow solid precipitates from solution. Combining the masses of the two isolated fractions gave a final yield (0.235 g, 49 % yield). Atomic composition of complex consistent with crystal structure.

CV (DMA) E$_{p,a}$ = +0.30 V (NHE). IR: ν(BH) = 2483 cm^{-1}, ν(NO) = 1535 cm^{-1}. ^{1}H-NMR (CDCl$_3$, δ, 20 °C): 8.19 (1H, d, Tp3/5), 8.08 (1H, d, Tp3/5), 7.67 (1H, d, Tp3/5), 7.64 (1H, d, Tp3/5), 7.58 (1H, d, Tp3/5), 7.27 (1H, d, Tp3/5), 6.27 (1H, t, Tp4), 6.17 (1H, t, Tp4), 6.12 (1H, t, Tp4), 2.74 (2H, overlapping m, H3 and H6), 2.64 (2H, overlapping m, H1 and H3), 2.48 (1H, m, H6), 1.87 (3H, m, PBu$_3$), 1.73 (3H, m, PBu$_3$), 1.79 (1H, m, H4/5), 1.76 (1H, m, H4/H5), 1.44 (2H, overlapping m, H4/H5), 1.35 (1H, m, H2), 1.21 (3H, m, PBu$_3$), 1.16 (3H, m,PBu$_3$), 0.96 (3H, m, PBu$_3$), 0.87 (3H, m, PBu$_3$), 0.78 (9H, t, J = 7.22, PBu$_3$). ^{31}P-NMR (CDCl$_3$, δ, 20 °C): -1.83 (J_{WP} = 276). ^{13}C-NMR (CDCl$_3$, δ, 25 °C): 145.0 (Tp3/5), 142.6 (Tp3/5), 140.6 (Tp3/5), 136.1 (Tp3/5), 135.4 (Tp3/5), 135.0 (Tp3/5), 136.1 (Tp3/5), 135.4 (Tp3/5), 135.0)Tp3/5), 106.3 (Tp4), 195.6 (Tp4), 105.4 (Tp4), 53.8 (C2, m, J_{WC} = 29.9), 52.4 (C1, m, J_{PC} = 11.0, J_{WC} =24.5), 29.6 (C6), 27.6 (C3), 25.1 (C4/5), 25.0 (PBu$_3$), 24.9 (PBu$_3$, J_{PC} =15.1), 24.7 (PBu$_3$, J_{PC} =11.8), 22.9 (PBu$_3$, J_{PC} =23.4),22.5 (C4/5), 13.88 (PBu$_3$).

Synthesis of WTp(NO)(PBu$_3$)(η^2-3,4-trifluoromethyl-benzenium) (10)

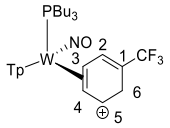

An in situ sample of **10** was prepared by chilling an NMR scale solution with MeCN-d_3 (~1/2 mL) of **4** (~ 30 mgs) to -30 °C over a period of 15 min. To this initially heterogeneous yellow solution was added 5 drops of HOTf that had also been chilled to -30 °C. Upon addition the reaction mixture turns to a homogeneous red solution and this sample was frozen in $N_{2(l)}$ and a ^{1}H NMR spectra was taken of this sample upon thawing at reduced temperatures.

^{1}H-NMR (MeCN-d_3, δ, 0 °C): 8.32 (1H, d, Tp3/5), 8.04 (1H, d, Tp3/5), 8.03 (1H, d, Tp3/5), 7.95 (1H, d, Tp3/5), 7.93 (1H, d, Tp3/5), 7.77 (1H, d, Tp3/5), 7.04 (2H, overlapping broad d, H2 and H5), 6.54 (1H, t, Tp4), 6.48 (1H, t, Tp4), 6.29 (1H, t, Tp4), 5.06 (1H, t, J = 6.75, H4), 4.26 (1H, buried, H3), 4.15 (1H, roofing d, J = 27.3, H6 syn/anti), 4.01 (1H, roofing d, J = 27.3, H6 syn/anti), 1.92 (3H, broad, PBu$_3$), 1.48 (3H, broad, PBu$_3$), 1.22 (3H, m, PBu$_3$), 1.16 (3H, m, PBu$_3$), 0.98 (3H, broad, PBu$_3$), 0.77 (9H, t, J = 7.60, PBu$_3$), 0.61 (3H, broad, PBu$_3$).

Synthesis of WTp(NO)(PBu$_3$)(η^2-3,4-(methyl-2-methyl-2-(5-(trifluoromethyl)cyclohexa-2,4-dien-1-yl)-propanoate)) (11)

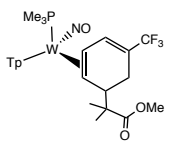

First **3** (0.802 g, 1.03 mmol) was dissolved in 3 mL of MeCN and chilled to -30 °C over a period of 15 min. After 15 min HOTf (0.241 g, 1.59 mmol) was added and upon addition the reaction mixture, initially a heterogeneous yellow solution turns to a homogeneous red reaction

mixture. This solution was allowed to sit at -30 ºC for 15 min and then methyl trimethylsilyl dimethylketene acetal (MTDA, 1.70 g, 9.77 mmol) was added to the reaction mixture and this was allowed to sit for 22 h at – 30 ºC. The next day a -30 ºC solution of triethylamine (1.00 g, 9.88 mmol) was added to the reaction mixture. The reaction mixture was then filtered through a medium 30 mL fritted disc that had been filled with ~ 3cm of silica and set in diethyl ether. The reaction mixture was eluted with diethyl ether until a lime green band began to elute through the column. Before collection the clear eluent was discarded and the lime green band was washed with ~60 mL of diethyl ether. The solvent was then removed in vacuo until a light green solid developed on the bottom of the flask and NMR analysis was performed in acetone-d_6 before the reaction was carried on to the synthesis of **15**. Crystals suitable for X-ray diffraction were grown in a mixture of acetone:chloroform at reduced temperatures and support the elemental composition of the complex.

^{1}H-NMR (acetone-d_6, δ, 25 ºC): 8.09 (1H, d, Tp3/5), 7.98 (1H, d, Tp3A), 7.95 (1H, d, Tp5C), 7.93 (1H, d, Tp3/5B), 7.84 (1H, d, Tp5A), 7.68 (1H, d, Tp3C), 7.17 (1H, broad s, H2), 6.39 (1H, t, Tp4B), 6.33 (2H, overlapping t, Tp4A/C), 3.42 (1H, d, J= 9.06, H5-syn), 3.17 (3H, OMe, s), 2.95 (1H, m, H3), 2.85 (1H, m, H6-syn), 2.02 (1H, d, J = 17.44, H6-anti), 1.92 (3H, m, PBu_3), 1.82 (3H, m, PBu_3), 1.25 (3H, m, PBu_3), 1.27 (3H, m, PBu_3), 1.09 (3H, m, PBu_3), 0.81 (3H, broad m, PBu_3), 0.77 (9H, t, J = 7.15, PBu_3), 1.23 (3H, s, Me), 1.16 (3H, s, Me). ^{31}P-NMR (acetone-d_6, δ, 25 ºC): -3.40 (J_{WP}= 269). ^{19}F-NMR (acetone-d_6, δ, 25 ºC): -66.36 (CF_3). ^{13}C-NMR (acetone-d_6, δ, 25 ºC): 178.7 (CO_2Me), 145.1 (Tp3/5), 142.2 (Tp3/5), 141.8 (Tp3/5), 137.9 (C2), 137.6 (Tp3/5), 137.2 (Tp3/5), 136.9(Tp3/5), 126.6 (CF_3, q, J_{CF} = 271), 116.7 (C1, q, J_{CF} = 29.5), 107.3 (Tp4), 107.1 (Tp4), 106.3 (Tp4), 55.1 (C4), 52.2 (C-Me$_2$), 51.1 (OMe), 47.3 (C3, d, J_{CP} = 10.4), 42.3 (C5), 25.8 (PBu_3), 25.0 (PBu_3, d, J_{PC} = 12.84), 23.8 (PBu_3, d, J_{PC} = 24.0), 23.5 (PBu_3), 22.3 (Me), 21.4 (Me), 13.9 (PBu_3).

Synthesis of methyl-2-methyl-2-(5-(trifluoromethyl)cyclohexa-2,4-dien-1-yl)-propanoate (12)

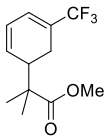

A solution of **11** in acetone-d_6 had its solvent removed in vacuo and was subsequently dissolved in 3 mL of $CDCl_3$. This solution was then added to a 1 mL solution of $NOPF_6$ (0.250g, 1.42 mmol) in $CDCl_3$ and upon addition of the solution of **11** the reaction mixture turned from a lime green color to a brown and finally to a yellow colored solution. This solution was then checked by ^{1}H NMR and upon observation that some of **11** still remained, the solution was then allowed to stir in a 4-dram vial and to this more $NOPF_6$ (0.330 g, 1.89 mmol) was added. Upon checking the reaction mixture by ^{1}H NMR again the absence of **11** was insured and the reaction mixture was purified with chromatography as has been previously reported.[38] Characterization matches the previously reported free organic and was isolated in 24% total yield (0.061 g, 0.246 mmol) starting from **4** (0.802 g, 1.03 mmol).

AUTHOR INFORMATION

Corresponding Authors

W. Dean Harman: wdh5z@virginia.edu
Daniel H. Ess: dhe@chem.byu.edu

Notes:
The authors declare no competing financial interest.

ACKNOWLEDGMENT

W.D.H is grateful for financial support from the National Institutes of Health (1R01GM132205). D.H.E. acknowledges the United States National Science Foundation Chemical Structure, Dynamics, and Mechanisms B (CSDM-B) Program for support under award CHE 1952420. We thank Brigham Young University and the Office of Research Computing, especially the Fulton Supercomputing Lab. A. S. thanks the BYU Department of Chemistry and Biochemistry for undergraduate research awards.

Supporting Information Available:

^{1}H and ^{13}C NMR spectra of selected compounds, DFT calculations, and crystallographic information for compounds **1**, **3A**, **4**, **6**, **10**, **11**. This material is available free of charge via the Internet at http://pubs.acs.org CCDC 1966807-1966811 and 1966813 contain the supplementary crystallographic data for this paper. These data can be obtained free of charge from The Cambridge Crystallographic Data Centre via www.ccdc.cam.ac.uk/structures

REFERENCES

1. Pony Yu, R.; Hesk, D.; Rivera, N.; Pelczer, I.; Chirik, P. J., Iron-catalysed tritiation of pharmaceuticals. *Nature* **2016**, *529*, 195-199.
2. Loh, Y. Y.; Nagao, K.; Hoover, A. J.; Hesk, D.; Rivera, N. R.; Colletti, S. L.; Davies, I. W.; MacMillan, D. W. C., Photoredox-Catalyzed Deuteration and Tritiation of Pharmaceutical Compounds. *Science* **2017**, *358*, 1182-1187.
3. Davies, H. M. L.; Beckwith, R. E. J., Catalytic Enantioselective C−H Activation by Means of Metal−Carbenoid-Induced C−H Insertion. *Chem. Rev.* **2003**, *103*, 2861-2904.
4. Topczewski, J. J.; Sanford, M. S., Carbon–hydrogen (C–H) bond activation at PdIV: a Frontier in C–H functionalization catalysis. *Chemical Science* **2015**, *6*, 70-76.
5. Jones, W. D., On the Nature of Carbon−Hydrogen Bond Activation at Rhodium and Related Reactions. *Inorganic Chemistry* **2005**, *44*, 4475-4484.
6. Balcells, D.; Clot, E.; Eisenstein, O., C—H Bond Activation in Transition Metal Species from a Computational Perspective. *Chem. Rev.* **2010**, *110*, 749-823.
7. Eisenstein, O.; Milani, J.; Perutz, R. N., Selectivity of C–H Activation and Competition between C–H and C–F Bond Activation at Fluorocarbons. *Chem. Rev.* **2017**, *117*, 8710-8753.
8. Gandeepan, P.; Müller, T.; Zell, D.; Cera, G.; Warratz, S.; Ackermann, L., 3d Transition Metals for C–H Activation. *Chem. Rev.* **2019**, *119*, 2192-2452.
9. Lersch, M.; Tilset, M., Mechanistic Aspects of C−H Activation by Pt Complexes. *Chem. Rev.* **2005**, *105*, 2471-2526.
10. Shilov, A. E.; Shul'pin, G. B., Activation of C−H Bonds by Metal Complexes. *Chem. Rev.* **1997**, *97*, 2879-2932.
11. Xue, X.-S.; Ji, P.; Zhou, B.; Cheng, J.-P., The Essential Role of Bond Energetics in C–H Activation/Functionalization. *Chem. Rev.* **2017**, *117*, 8622-8648.
12. Jones, W. D., Isotope effects in C-H bond Activation Reactions by Transition Metals. *Accounts of chemical research* **2003**, *36*, 140-146.
13. Churchill, D. G.; Janak, K. E.; Wittenberg, J. S.; Parkin, G., Normal and Inverse Primary Kinetic Deuterium Isotope Effects for C−H Bond Reductive Elimination and Oxidative Addition Reactions of Molybdenocene and Tungstenocene Complexes:
14. Stoutland, P. O.; Bergman, R. G., Insertion of Iridium into the Carbon-Hydrogen Bonds of Alkenes: the π-complex Cannot be an Intermediate. *J. Am. Chem. Soc.* **1985**, *107*, 4581-4582.
15. Solomon, R. G.; Kochi, J. K., Cationic Benzene and Olefin Complexes of Copper(I) Trifluoromethanesulphonate. *J. Chem. Soc., Comm.* **1972**, 559-560.

16. Norris, C. M.; Reinartz, S.; White, P. S.; Templeton, J. L., Barriers for Arene C−H Bond Activation in Platinum(II) η^2-Arene Intermediates. *Organometallics* **2002**, *21*, 5649-5656.
17. Liebov, B. K.; Harman, W. D., Group 6 Dihapto-Coordinate Dearomatization Agents for Organic Synthesis. *Chem. Rev.* **2017**, *117*, 13721-13755.
18. Tagge, C. D.; Bergman, R. G., Synthesis, X-ray Structure Determination, and Reactions of (Pentamethylcyclopentadienyl)(nitrosyl)ruthenium η^2-Arene Complexes. *J. Am. Chem. Soc.* **1996**, *118*, 6908-6915.
19. Driver, T. G.; Williams, T. J.; Labinger, J. A.; Bercaw, J. E., C−H Bond Activation by Dicationic Platinum(II) Complexes. *Organometallics* **2007**, *26*, 294-301.
20. Sweet, J. R.; Graham, W. A. G., Cationic η^2-arene Complexes of Rhenium in Carbon-Hydrogen Bond Activation. *J. Am. Chem. Soc.* **1983**, *105*, 305-306.
21. Jones, W. D.; Dong, L., Direct Observation of η^2-Arene Complexes of [(C_5Me_5)Rh(PMe_3)]. *J. Am. Chem. Soc.* **1989**, *111*, 8722-8723.
22. Chin, R. M.; Dong, L.; Duckett, S. B.; Partridge, M. G.; Jones, W. D.; Perutz, R. N., Control of η^2-coordination vs. carbon-hydrogen bond activation by rhodium: the role of aromatic resonance energies. *J. Am. Chem. Soc.* **1993**, *115*, 7685-7695.
23. Harman, W. D., The Activation of Aromatic Molecules with Pentaammineosmium(II). *Chem. Rev.* **1997**, *97*, 1953-1978.
24. Keane, J. M.; Harman, W. D., A New Generation of Pi-Basic Dearomatization Agents. *Organometallics* **2005**, *24*, 1786-1798.
25. Liu, W.; Welch, K.; Trindle, C. O.; Sabat, M.; Myers, W. H.; Harman, W. D., Facile Intermolecular Aryl−F Bond Cleavage in the Presence of Aryl C−H Bonds: Is the η^2-Arene Intermediate Bypassed? *Organometallics* **2007**, *26*, 2589-2597.
26. Fukui, K., The path of chemical reactions - the IRC approach. *Accounts of Chemical Research* **1981**, *14*, 363-368.
27. Welch, K. D.; Harrison, D. P.; Lis, E. C.; Liu, W.; Salomon, R. J.; Harman, W. D.; Myers, W. H., Large-Scale Syntheses of Several Synthons to the Dearomatization Agent {TpW(NO)(PMe_3)} and Convenient Spectroscopic Tools for Product Analysis. *Organometallics* **2007**, *26*, 2791-2794.
28. Zhao, Y.; Truhlar, D. G., The M06 Suite of Density Functionals for Main Group Thermochemistry, Thermochemical Kinetics, Noncovalent Interactions, Excited States, and Transition Elements: Two New Functionals and Systematic Testing of Four M06-class Functionals and 12 Other Functionals. *Theoretical Chemistry Accounts* **2008**, *120*, 215-241.
29. Peverati, R.; Truhlar, D. G., Improving the Accuracy of Hybrid Meta-GGA Density Functionals by Range Separation. *The Journal of Physical Chemistry Letters* **2011**, *2*, 2810-2817.
30. Frisch, M. J.; Trucks, G. W.; Schlegel, H. B.; Scuseria, G. E.; Robb, M. A.; Cheeseman, J. R.; Scalmani, G.; Barone, V.; Petersson, G. A.; Nakatsuji, H.; Li, X.; Caricato, M.; Marenich, A. V.; Bloino, J.; Janesko, B. G.; Gomperts, R.; Mennucci, B.; Hratchian, H. P.; Ortiz, J. V.; Izmaylov, A. F.; Sonnenberg, J. L.; Williams; Ding, F.; Lipparini, F.; Egidi, F.; Goings, J.; Peng, B.; Petrone, A.; Henderson, T.; Ranasinghe, D.; Zakrzewski, V. G.; Gao, J.; Rega, N.; Zheng, G.; Liang, W.; Hada, M.; Ehara, M.; Toyota, K.; Fukuda, R.; Hasegawa, J.; Ishida, M.; Nakajima, T.; Honda, Y.; Kitao, O.; Nakai, H.; Vreven, T.; Throssell, K.; Montgomery Jr., J. A.; Peralta, J. E.; Ogliaro, F.; Bearpark, M. J.; Heyd, J. J.; Brothers, E. N.; Kudin, K. N.; Staroverov, V. N.; Keith, T. A.; Kobayashi, R.; Normand, J.; Raghavachari, K.; Rendell, A. P.; Burant, J. C.; Iyengar, S. S.; Tomasi, J.; Cossi, M.; Millam, J. M.; Klene, M.; Adamo, C.; Cammi, R.; Ochterski, J. W.; Martin, R. L.; Morokuma, K.; Farkas, O.; Foresman, J. B.; Fox, D. J. *Gaussian 16 Rev. C.01*, Wallingford, CT, 2016.
31. Marenich, A. V.; Cramer, C. J.; Truhlar, D. G., Universal Solvation Model Based on Solute Electron Density and on a Continuum Model of the Solvent Defined by the Bulk Dielectric Constant and Atomic Surface Tensions. *J. Phys. Chem. B* **2009**, *113*, 6387-6396.
32. Graham, P. M.; Meiere, S. H.; Sabat, M.; Harman, W. D., Dearomatization of Benzene, Deamidization of N,N-Dimethylformamide, and a Versatile New Tungsten π Base. *Organometallics* **2003**, *22*, 4364-4366.
33. Harrison, D. P.; Nichols-Nielander, A. C.; Zottig, V. E.; Strausberg, L.; Salomon, R. J.; Trindle, C. O.; Sabat, M.; Gunnoe, T. B.; Iovan, D. A.; Myers, W. H.; Harman, W. D., Hyperdistorted Tungsten Allyl Complexes and Their Stereoselective Deprotonation to Form Dihapto-Coordinated Dienes. *Organometallics* **2011**, *30*, 2587-2597.
34. The conversion of **2s** to the η^2 arene **2** or its microscopic reverse can happen in two different directions (cw and ccw) with corresponding transition states (TS2) slightly differing in energy. See SI for details.
35. Tobisch, S.; Ziegler, T., Catalytic Linear Oligomerization of Ethylene to Higher α-Olefins: Insight into the Origin of the Selective Generation of 1-Hexene Promoted by a Cationic Cyclopentadienyl-Arene Titanium Active Catalyst. *Organometallics* **2003**, *22*, 5392-5405.
36. Contreras-Garcia, J.; Johnson, E. R.; Keinana, S.; R., C.; Piquemal, J. P.; Beratan, D. N.; Yang, W., NCIPLOT: A Program for Plotting Noncovalent Interaction Regions. *J. Chem. Theory Comput.* **2011**, *7*, 625-632.
37. Khaliullin, R. Z.; Cobar, E. A.; Lochan, R. C.; Bell, A. T.; Head-Gordon, M., Unravelling the Origin of Intermolecular Interactions Using Absolutely Localized Molecular Orbitals. *J. Phys. Chem. A* **2007**, *111*, 8753-8765.
38. Shao, Y.; Gan, Z.; Epifanovsky, E.; Gilbert, A. T. B.; Wormit, M.; Kussmann, J.; Lange, A. W.; Behn, A.; Deng, J.; Feng, X.; Ghosh, D.; Horn, M. G. P. R.; Jacobson, L. D.; Kaliman, I.; Khaliullin, R. Z.; Kús, T.; Landau, A.; Liu, J.; Proynov, E. I.; Rhee, Y. M.; Richard, R. M.; Rohrdanz, M. A.; Steele, R. P.; Sundstrom, E. J.; III, H. L. W.; Zimmerman, P. M.; Zuev, D.; Albrecht, B.; Alguire, E.; Austin, B.; Beran, G. J. O.; Bernard, Y. A.; Berquist, E.; Brandhorst, K.; Bravaya, K. B.; Brown, S. T.; Casanova, D.; Chang, C.-M.; Chen, Y.; Chien, S. H.; Closser, K. D.; Crittenden, D. L.; Diedenhofen, M.; Jr., R. A. D.; Dop, H.; Dutoi, A. D.; Edgar, R. G.; Fatehi, S.; Fusti-Molnar, L.; Ghysels, A.; Golubeva-Zadorozhnaya, A.; Gomes, J.; Hanson-Heine, M. W. D.; Harbach, P. H. P.; Hauser, A. W.; Hohenstein, E. G.; Holden, Z. C.; Jagau, T.-C.; Ji, H.; Kaduk, B.; Khistyaev, K.; Kim, J.; Kim, J.; King, R. A.; Klunzinger, P.; Kosenkov, D.; Kowalczyk, T.; Krauter, C. M.; Lao, K. U.; Laurent, A.; Lawler, K. V.; Levchenko, S. V.; Lin, C. Y.; Liu, F.; Livshits, E.; Lochan, R. C.; Luenser, A.; Manohar, P.; Manzer, S. F.; Mao, S.-P.; Mardirossian, N.; Marenich, A. V.; Maurer, S. A.; Mayhall, N. J.; Oana, C. M.; Olivares-Amaya, R.; O'Neill, D. P.; Parkhill, J. A.; Perrine, T. M.; Peverati, R.; Pieniazek, P. A.; Prociuk, A.; Rehn, D. R.; Rosta, E.; Russ, N. J.; Sergueev, N.; Sharada, S. M.; Sharmaa, S.; Small, D. W.; Sodt, A.; Stein, T.; Stück, D.; Su, Y.-C.; Thom, A. J. W.; Tsuchimochi, T.; Vogt, L.; Vydrov, O.; Wang, T.; Watson, M. A.; Wenzel, J.; White, A.; Williams, C. F.; Vanovschi, V.; Yeganeh, S.; Yost, S. R.; You, Z.-Q.; Zhang, I. Y.; Zhang, X.; Zhou, Y.; Brooks, B. R.; Chan, G. K. L.; Chipman, D. M.; Cramer, C. J.; III, W. A. G.; Gordon, M. S.; Hehre, W. J.; Klamt, A.; III, H. F. S.; Schmidt, M. W.; Sherrill, C. D.; Truhlar, D. G.; Warshel, A.; Xua, X.; Aspuru-Guzik, A.; Baer, R.; Bell, A. T.; Besley, N. A.; Chai, J.-D.; Dreuw, A.; Dunietz, B. D.; Furlani, T. R.; Gwaltney, S. R.; Hsu, C.-P.; Y. Jung, J. K.; Lambrecht, D. S.; Liang, W.; Ochsenfeld, C.; Rassolov, V. A.; Slipchenko, L. V.; Subotnik, J. E.; Voorhis, T. V.; Herbert, J. M.; Krylov, A. I.; Gill, P. M. W.; Head-Gordon, M., Advances in molecular quantum chemistry contained in the Q-Chem 4 program package. *Molecular Physics* **2015**, *113*, 184-215.
39. Ma, X.; Hase, W. L., Perspective: chemical dynamics simulations of non-statistical reaction dynamics. *Philosophical Transactions of the Royal Society A: Mathematical, Physical and Engineering Sciences* **2017**, *375*, 20160204.
40. Bonnington, K. J.; Zhang, F.; Moustafa, M. M. A. R.; Cooper, B. F. T.; Jennings, M. C.; Puddephatt, R. J., Activation of Anisole by Organoplatinum(II) Complexes: Evidence for Rate-Determining C–H Activation. *Organometallics* **2012**, *31*, 306-317.
41. Brooks, B. C.; Meiere, S. H.; Friedman, L. A.; Carrig, E. H.; Gunnoe, T. B.; Harman, W. D., Interfacial and Intrafacial Linkage Isomerizations of Rhenium Complexes with Aromatic Molecules. *J. Am. Chem. Soc.* **2001**, *123*, 3541-3550.
42. Harman, W. D.; Sekine, M.; Taube, H., Substituent effects on .eta.2-coordinated arene complexes of pentaammineosmium(II). *Journal of the American Chemical Society* **1988**, *110*, 5725-5731.
43. Seidel, R. W.; Goddard, R., Anisole at 100 K: the first crystal structure determinationDedicated to Professor Wolfgang Klaui on the occasion of his 70th birthday. *Acta Crystallographica Section C* **2015**, *71*, 664-666.
44. Hirao, H.; Ohwada, T., Theoretical Study of Reactivities in Electrophilic Aromatic Substitution Reactions: Reactive Hybrid Orbital Analysis. *The Journal of Physical Chemistry A* **2003**, *107*, 2875-2881.

45. Sharp, W. B.; Legzdins, P.; Patrick, B. O., O-Protonation of a Terminal Nitrosyl Group To Form an η1-Hydroxylimido Ligand. *J. Am. Chem. Soc.* **2001**, *123*, 8143-8144.
46. Myers, J. T.; Smith, J. A.; Dakermanji, S. J.; Wilde, J. H.; Wilson, K. B.; Shivokevich, P. J.; Harman, W. D., Molybdenum(0) Dihapto-Coordination of Benzene and Trifluorotoluene: The Stabilizing and Chemo-Directing Influence of a CF3 Group. *J. Am. Chem. Soc.* **2017**, *139* (33), 11392-11400.
47. Harrison, D. P.; Welch, K. D.; Nichols-Nielander, A. C.; Sabat, M.; Myers, W. H.; Harman, W. D., Efficient Synthesis of an η2-Pyridine Complex and a Preliminary Investigation of the Bound Heterocycle's Reactivity. *J. Am. Chem. Soc.* **2008**, *130*, 16844-16845.
48. Strausberg, L.; Li, M.; Harrison, D. P.; Myers, W. H.; Sabat, M.; Harman, W. D., Exploiting the o-Quinodimethane Nature of Naphthalene: Cycloaddition Reactions with η2-Coordinated Tungsten–Naphthalene Complexes. *Organometallics* **2013**, *32*, 915-925.
49. Delafuente, D. A.; Myers, W. H.; Sabat, M.; Harman, W. D., Tungsten(0) η^2-Thiophene Complexes: Dearomatization of Thiophene and Its Facile Oxidation, Protonation, and Hydrogenation. *Organometallics* **2005**, *24*, 1876-1885.
50. Belt, S. T.; Dong, L.; Duckett, S. B.; Jones, W. D.; Partridge, M. G.; Perutz, R. N., Control of η^2-arene coordination and C–H bond activation by cyclopentadienyl complexes of rhodium. *Journal of the Chemical Society, Chemical Communications* **1991**, 266-269.
51. Crabtree, R. H., *The Organometallic Chemistry of the Transition Metals* 7th Ed. John Wiley: New York, 2019.
52. Wilson, K. B.; Myers, J. T.; Nedzbala, H. S.; Combee, L. A.; Sabat, M.; Harman, W. D., Sequential Tandem Addition to a Tungsten–Trifluorotoluene Complex: A Versatile Method for the Preparation of Highly Functionalized Trifluoromethylated Cyclohexenes. *J. Am. Chem. Soc.* **2017**, *139*, 11401-11412.

TOC